UNITED STATES DEPARTMENT OF THE INTERIOR
GEOLOGICAL SURVEY

Earthquake Hazards in the Pacific Northwest of the United States

Compiled by
A. M. Rogers
T.J. Walsh
W.J. Kockelman
G.R. Priest

ACTIVE STRIKE-SLIP FAULTING AND FOLDING OF THE CASCADIA PLATE BOUNDARY AND FOREARC IN CENTRAL AND NORTHERN OREGON

BY CHRIS GOLDFINGER[1], LAVERNE D. KULM[2], ROBERT S. YEATS[1], BRUCE APPELGATE[3], MARY E. MACKAY[3], AND GUY R. COCHRANE[4]

Open-File Report 91-441-S

[1] Department of Geosciences, Oregon State University, Corvallis Oregon 97331
[2] College of Oceanography, Oregon State University, Corvallis Oregon 97331
[3] SOEST, University of Hawaii, Honolulu Hawaii 96822
[4] Earth Sciences, University of California at Santa Cruz, 95064

1991

Foreword

This paper is one of a series dealing with earthquake hazards of the Pacific Northwest, primarily in western Oregon and western Washington. This research represents the efforts of U.S. Geological Survey, university, and industry scientists in response to the Survey initiatives under the National Earthquake Hazards Reduction Program. Subject to Director's approval, these papers will appear collectively as U.S. Geological Survey Professional Paper 1560, tentatively titled "Assessing Earthquake Hazards and Reducing Risk in the Pacific Northwest." The U.S. Geological Survey Open-File series will serve as a preprint for the Professional Paper chapters that the editors and authors believe require early release. A single Open-File will also be published that includes only the abstracts of those papers not included in the pre-release. The papers to be included in the Professional Paper are:

Introduction

Rogers, A.M., Walsh, T.J., Kockelman, W.J., and Priest, G.R., "Earthquake hazards in the Pacific Northwest: An overview

Tectonic Setting

Paleoseismicity

Adams, John, "Great earthquakes recorded by turbidites off the Oregon-Washington margin"

Atwater, B.F., "Coastal evidence for great earthquakes in western Washington"

Nelson, A.R., and Personius, S. F., "The potential for great earthquakes in Oregon and Washington: An overview of recent coastal geologic studies and their bearing on segmentation of Holocene ruptures, central Cascadia subduction zone"

Peterson, C. D., and Darienzo, M. E., "Discrimination of climatic, oceanic, and tectonic forcing of marsh burial events from Alsea Bay, Oregon, U.S.A."

Tectonics/Geophysics

Goldfinger, C., Kulm, L.D., Yeats, R.S., Appelgate, B., MacKay, M., and Cochrane, G., "Active strike-slip faulting and folding in the Cascadia plate boundary and forearc, in central and northern Oregon"

Ma, Li, Crosson, R.S., and Ludwin, R.S., "Focal mechanisms of western Washington earthquakes and their relationship to regional tectonic stress"

Snavely, P. D., Jr., and Wells, R.E., "Cenozoic evolution of the continental margin of Oregon and Washington"

Weaver, C. S., and Shedlock, K. M., "Estimates of seismic source regions from considerations of the earthquake distribution and regional tectonics"

Yeats, R.S., Graven, E.P., Werner, K.S., Goldfinger, C., and Popowski, T.A., "Tectonic setting of the Willamette Valley, Oregon"

Earthquake Hazards

Ground Motion Prediction

Cohee, B.P., Somerville, P.G., and Abrahamson, N.A., "Ground motions from simulated M_W=8 Cascadia earthquakes"

King, K.W., Carver, D.L., Williams, R.A., and Worley, D.M., "Site response studies in west and south Seattle, Washington"

Madin, I. P., "Earthquake-hazard geology maps of the Portland metropolitan area, Oregon"

Silva, W.J., Wong, I.G., and Darragh, R.B., "Engineering characterization of strong ground motions with applications to the Pacific Northwest"

Ground Failure

Chleborad, A. F., and Schuster, R. L., "Earthquake-induced ground failure associated with the April 13, 1949, and April 29, 1963, Puget Sound area, Washington, earthquakes"

Grant, W. P., Perkins, W. J., and Youd, L., "Liquefaction susceptibility maps for Seattle, Washington North and South Quadrangles

Earthquake Risk Assessment

Wang, Leon R.L., Wang, Joyce C.C., and Ishibashi, Isao, "GIS applications in seismic loss estimation model for Portland, Oregon water and sewer systems"

Implementation

Kockelman, W. J., "Techniques for reducing earthquake hazards--An introduction"

Booth, D.B., and Bethel, J.P., "Approaches for seismic hazard mitigation by local governments--An example from King County, Washington"

May, P.J., "Earthquake risk reduction prospects for the Puget Sound and Portland Areas"

Perkins, J.B., and Moy, K.K., "Liability for earthquake hazards or losses and its impacts on Washington's cities and counties"

Preuss, Jane, and Hebenstreit, G. T., "Integrated hazard assessment for a coastal community: Grays Harbor"

Contents

Abstract....1
Introduction....1
Methods....2
Strike-slip Faults on the Juan de Fuca Plate....2
The Wecoma Fault....3
Age, Net Slip, and Average Slip Rate of the Wecoma Fault....4
Abyssal Plain Stratigraphy....4
Timing Constraints....4
Fault Restoration....5
Late Pleistocene-Holocene Slip Rate....6
Intersection of Wecoma Fault and the Accretionary Wedge....6
Influence of the Wecoma Fault on the Accretionary Wedge....6
Discussion....8
Fault Orientation....8
Strike-Slip Faults and the Accretionary Wedge....8
Implications for Cascadia Convergence....9
Conclusions....10
Acknowledgments....10
References....11
Figure Captions....13

Illustrations

Figure 1. Plate tectonic configuration of the Juan de Fuca-North American convergence zone....15
Figure 2. Trackline map showing the location of all seismic reflection profiles used in this study....16
Figure 3. Seismic-reflection trackline map and bathymetry in the detailed study area....17
Figure 4. Generalized structure map of the northern and central Oregon margin....18
Figure 5. Perspective fishnet plot of SeaBeam swath bathymetry off central and northern Oregon....19
Figure 6. Mosaic of SeaMARC 1A 5 kilometer swaths in the vicinity of the Wecoma fault....20
Figure 7. Structure map of the western portion of the Wecoma fault and frontal accretionary wedge....21
Figure 8. Migrated MCS line 37 crossing of the Wecoma fault between the pressure ridge and the deformation front and interpretation of line 37....22
Figure 9. Migrated MCS line 45 crossing of the Wecoma fault and the pressure ridge anticline....23
Figure 10. Composite block diagram of the pressure ridge area and intersection between the Wecoma fault and the deformation front....24
Figure 11. Line drawing of a single-channel reflection profile (OSU cruise YALOC 70, Leg 5)....25
Figure 12. Lithology and coiling directions of Globigerina pachyderma in cores from DSDP site 174....26
Figure 13. Cartoon illustrating the method used in fault reconstruction....27
Figure 14. Isopach plot of abyssal plain unit 2....28
Figure 15. High-resolution SeaMARC 1A sidescan image of Wecoma fault....29
Figure 16. Structural interpretation of the intersection zone and pop-up structure....30
Figure 17. Block diagram illustrating structure of the pop-up....31
Figure 18. ALVIN submersible tracklines....32
Figure 19. Sandy siltstone samples collected with ALVIN....33
Figure 20. SeaMARC 1A sidescan image of the Wecoma fault crossing the accretionary wedge. and interpretation showing offset of anticlinal axis....34-35
Figure 21. Unmigrated 24-channel seismic profile of the Wecoma fault on the lower continental slope and interpreted profile....36
Figure 22. SeaBeam bathymetry and structure of a portion of the central continental slope....37
Figure 23. A) Location map of seismic profiles....38
Figure 23. B) Line drawing of part of Shell line 7380....39
Figure 23. C) Unmigrated single-channel seismic profile of a strike-slip fault within the Wecoma deformation zone on the upper continental slope and interpreted profile....40
Figure 24. SeaBeam bathymetry perspective view along the strike of the Wecoma fault....41
Figure 25. Vector diagram of the inferred local effect of Wecoma fault slip on the plate convergence vector....42

ABSTRACT

Three WNW-trending left-lateral strike-slip faults on the abyssal plain off northern and central Oregon between 44° 40' N and 45° 12' N latitude have been mapped using seismic reflection, sidescan sonar, ALVIN submersible dives, and SeaBeam bathymetry. These oblique faults intersect the north-south striking structures of the active accretionary wedge. The faults cut the oceanic lithosphere of the subducting Juan de Fuca plate and appear to cross the plate boundary. The best studied of these, the Wecoma fault, extends 18 km northwestward across the abyssal plain from the deformation front. Displacement on this fault is 5.5 ± 0.8 km at the deformation front, decreasing to zero at the northwestern fault tip based upon piercing-point offset. The Wecoma fault has been active for approximately 600 ± 50 ka, with an average slip rate of 7-10 mm/yr. The latest Pleistocene-Holocene slip rate is 5-12 mm/yr. These faults are active, as indicated by the offset of the youngest sedimentary units, the presence of surficial fault scarps, and the venting of deeply sourced fluids. The Wecoma fault intersects the deformation front in a complex structural zone consisting of fault-bounded pop-ups, an embayment in the deformation front, and a local reversal of vergence in the basal thrust of the accretionary wedge. Fault B is also associated with an abrupt change in vergence direction of the basal accretionary thrust. Linear gullies and scarps in the Wecoma fault zone extend into the first several thrust ridges of the continental slope, suggesting that this fault remains active beneath the accretionary wedge. Changes in fold orientation and amount of shortening in the initial 3-4 thrust ridges of the accretionary wedge suggest that the strike-slip faults have influenced the development of coeval accretionary-wedge structures through differential slip of the downgoing plate. Several WNW-trending deformation zones have been mapped on the continental slope off northern and central Oregon. The deformation zones are composed of WNW-trending linear scarps, en-echelon NW- to WNW-trending folds, and left-stepping and sigmoidally bent folds. Oblique folds are commonly fault-propagation and fault-bend folds developed above high-angle faults. Some of these active faults and folds striking NNW to WNW are re-folding somewhat older north- and NNE-trending folds. Deformation in these zones is consistent with a left-lateral sense of shear. Three of these deformation zones lie along the landward projections of the three abyssal-plain strike-slip faults, while at least one, and possibly several others are restricted to the continental slope. We postulate that the deformation zones may either be shear zones developed in the upper plate above the subducted strike-slip faults, or that strike-slip faulting in the upper plate has propagated seaward into the subducting plate.

INTRODUCTION

The Cascadia subduction zone off Oregon and Washington may be one of the best studied subduction zones in the world. Its proximity to major U.S. ports, and three decades of study by oceanographic institutions, government agencies, and industry have provided an extensive data set for use in geological and geophysical investigations. In recent years, attention has been focused on the anomalous seismic quiescence of much of the Cascadia margin in comparison to other subduction zones. The moderate convergence rate of 40 mm/yr directed 062° (calculated from JDF-NAM Euler vector of DeMets and others, 1990), and the relative youth of the subducting lithosphere (9-10 Ma according to Wilson and others, 1984) should characterize the Cascadia subduction zone as a Chilean-type margin (Heaton and Kanamori, 1984). Since most Chilean-type margins have experienced great earthquakes in historic times, the Juan de Fuca-North American plate boundary should also be capable of generating great earthquakes. Geological evidence for great earthquakes has been inferred from buried marsh deposits of the coastal bays of Washington (Atwater, 1987; Atwater and Yamaguchi, 1991), Oregon (Darienzo and Peterson, 1990), and northern California (Carver and others, 1989; Clarke and Carver, 1989; Vick, 1988). Rapid co-seismic submergence accompanied by tsunamis is inferred from peat layers overlain by marine sands (Atwater, 1987). Presently, the Oregon Cascadia margin may have the lowest incidence of instrumental plate-boundary seismicity of any subduction zone. Although earthquakes in the upper and lower plates are well monitored by the University of Washington seismic network, no thrust-type earthquakes at any magnitude level have been located on the plate interface (Ludwin and others, 1989). The absence of historic great earthquakes in Cascadia can be explained by long recurrence intervals of 300 to 1000 years or more (Adams, 1990; Atwater, 1987; Darienzo and Peterson, 1990; Atwater and Yamaguchi, 1991; Carver and others, 1989), yet the Cascadia plate interface nonetheless remains singularly quiet among the world's convergent margins.

The low seismicity of the Cascadia subduction zone has led investigators to explore a variety of hypotheses to explain the apparent seismic gap along the Cascadia margin (Ando and Balasz, 1979; Sykes, 1989; West and McCrumb, 1988). Our investigation of the structure of the plate boundary and forearc offshore Oregon arose in part from the discovery of several oblique strike-slip faults in the abyssal plain off north-central Oregon. These faults cut the downgoing Juan de Fuca plate and cross the plate boundary, extending some distance into the overriding North American plate. To our knowledge, faults of this type have not previously been described from other subduction zones around the world, although strike-slip faulting restricted to the upper plate has been described in both orthogonal and oblique convergent settings (Lewis and others, 1988 and references therein; Geist and others, 1988).

Their discovery is almost certainly the result of the increased resolution in sea-floor mapping tools in recent years, but these faults may also represent something unique about the Cascadia convergent margin. Their discovery suggests the possibility that detailed structural investigations may offer new information about oblique subduction in general and Cascadia in particular.

The purpose of this paper is to investigate and document the structural evolution of the Wecoma fault, the largest and best known of three strike-slip faults discovered on the abyssal plain off Oregon, and to relate this fault to new mapping of active tectonic features of the continental slope. The long-term goal of this work is to better define the active tectonics of the Cascadia subduction zone, and thereby develop a better understanding of the regional tectonics and seismic hazards of the Pacific Northwest. We conclude with a discussion of possible origins and implications for plate-boundary processes of the oblique faults and folds we have mapped within the Cascadia convergent margin.

METHODS

We are studying the submerged plate boundary and forearc region off Oregon and Washington (fig. 1) using SeaMARC 1A and GLORIA sidescan sonar imagery, SeaBeam swath bathymetry, ALVIN submersible observations, and a dense network of single-channel and multichannel seismic (MCS) surveys. We are mapping the Oregon-Washington plate boundary and submarine forearc at a scale of 1:500,000. We have used approximately 30,000 km of seismic-reflection profiles collected by Oregon State University, University of California at Santa Cruz, University of Hawaii, University of Washington, Scripps Institution of Oceanography, U.S.G.S., N.O.A.A., and the oil industry (fig. 2). The profiles vary widely in quality, depth of penetration, and navigational accuracy, ranging from single-channel sparker records navigated with Loran-A, to 144-channel digital profiles navigated with GPS (Global Positioning System). Partially in preparation for Ocean Drilling Program Leg 146, a site survey consisting of closely-spaced high-resolution multichannel seismic lines, SeaMARC 1A sidescan mapping, SeaBeam swath bathymetry, and Alvin submersible dives focused on the plate boundary and accretionary wedge at the proposed drilling sites near 45° N latitude. (fig. 3). Within this 6000 km^2 area we were able to map submarine structures in considerable detail.

Within the detailed study area (fig. 3), the 144-channel reflection profiles were navigated with GPS, and position information from these lines is used as the datum for mapping that portion of the study area. Processing through time migration was carried out at the University of Hawaii. Several other U.S.G.S. 24-channel and OSU single-channel lines also constrain the structural interpretations. The sidescan and bathymetric surveys were navigated with a combination of GPS and Transit satellite navigation, with Loran C tracking used between satellite fixes. Navigation of the deep-towed sidescan fish was done by the method described by Appelgate (1988). Where spatial misfits occur, we have adjusted the sidescan data to best fit the GPS navigated MCS lines or the SeaBeam bathymetry where appropriate. SeaMarc 1A sidescan data were collected with a deep-towed 30 kHz system capable of imaging a 2 km or a 5 km swath width, with spatial resolutions of 1 and 2.5 meters, respectively. A magnetometer attached to the towfish recorded total field intensity over the sidescan tracks. Our mode of operation during sidescan surveys was to cover the study area at the wider 5 km swath width, then return to areas of interest and conduct detailed surveys using the higher-resolution 2 km swath. Sidescan processing, which included geometrical and speed corrections, correction for towfish position, orthorectification of image pixels to a latitude/longitude grid, and image enhancement (as described in Appelgate, 1988) was carried out at the N.O.A.A. image processing facility in Newport, Oregon. Outside the detailed study area, navigational accuracy was more variable. Loran A navigated profiles have maximum errors on the order of 1-3 kilometers, Loran C errors are approximately 0-1.5 km, and Transit satellite errors range from near zero up to hundreds of meters. The dense coverage of reflection profiles allowed adjustment of older lines where crossed by satellite-navigated lines.

STRIKE-SLIP FAULTS ON THE JUAN DE FUCA PLATE

Along the central and northern Oregon convergent margin, three WNW-trending left-lateral strike-slip faults (Wecoma fault, faults B and C, fig. 4) extend from the base of the continental slope 10-18 km northwestward across the abyssal plain. (*A note here concerning mapping conventions used in this paper: we show offsets across faults only where they can be demonstrated with existing data. Other offsets that might be expected, but are not demonstrated, are not shown.)* First imaged using SeaMARC 1A sidescan sonar in 1986, these faults were surveyed in detail in 1989 using a narrow-swath, high-resolution survey (Appelgate and others, 1992), and were crossed several times by multichannel seismic (MCS) profiles shot in 1989. In reflection profiles on the abyssal plain, the three faults show vertical separation of both the oceanic basement and the 2-3 km thick overlying sedimentary section (Appelgate and others, 1992; MacKay and others, 1992; this study). The three faults strike 290° to 295°, and all three are primarily strike-slip with a minor up-to-the-north component of displacement as evidenced by offset surface and subsurface features. In this paper we discuss primarily the Wecoma fault, since this fault is better covered

by seismic and sidescan surveys. Faults B and C appear to be similar in structural style to the Wecoma fault, but the more sparse data available on these faults presently precludes as detailed an assessment of them.

The Wecoma Fault

The Wecoma fault is the longest and best developed of the three strike-slip faults on the abyssal plain (fig. 4). A perspective fishnet diagram of the SeaBeam bathymetry shows the general physiography of the Wecoma fault, its associated structures, and the adjacent abyssal plain and accretionary wedge (fig. 5). A SeaMARC-IA sidescan mosaic (fig. 6) shows the surface trace and morphologic fea tures associated with the Wecoma fault and the complex intersection of the fault with the deformation front. We have integrated all of the available geophysical data in a structure map of the Wecoma fault on the abyssal plain and adjacent frontal accretionary wedge (fig. 7). Migrated multichannel seismic (MCS) profiles of the Wecoma fault reveal that it is nearly vertical, in places consisting of a main strand with little other deformation (figs. 8 A and B), and in others characterized by an upward branching positive flower structure (fig. 9) as defined by Harding and others (1985). Blocks within the flower structure mostly show minor reverse motion. In both seismic and sidescan records on the abyssal plain the displacement and surface expression of the Wecoma fault diminish toward the northwest. On the high-resolution 2 km sidescan swath, the trace of the fault was lost approximately 18 km WNW of the deformation front. A MCS record (line 33; fig. 3) crosses the along-strike projection of the fault 7 km WNW of the point at which the scarp disappeared on the 2 km sidescan record. At the projected location, only minor deformation is seen, suggesting that this line crosses near the fault tip. Two other crossing reflection profiles, located 3.7 and 5.5 km west of the line 33 crossing, show that the fault does not extend west of 125° 41' W (see fig. 3 for location).

Seismic-reflection profiles indicate that the Wecoma fault is a structural break in the downgoing Juan de Fuca plate. On line 37 (fig. 8 A and B) vertical separation of the basaltic basement is apparent both near the deformation front and beneath the pressure ridge, the NE block upthrown (Appelgate and others, 1992; this study). While the vertical separation of the basement seen in figure 8 is not large, identical vertical separation is also observed in the overlying stratigraphic units. A corresponding basement offset is required to produce the vertical separation of the sediments, such that the observed basement offset cannot be a hummock on the basement surface.

The overall strike of the Wecoma fault from the base of the slope to its northwestern terminus is 293°, extending 18 kilometers across the abyssal plain from the deformation front. The trace takes a gentle southward bend 7 km northwest of the deformation front, then abruptly terminates along the southern boundary of a structural upwarp (pressure ridge, PR, figs. 6, 7 and 9). Displacement is taken up by a second northwest trending right-stepping segment that originates on the northern flank of the upwarp, and strikes northwest to its terminus (figs. 6 and 7; see also Appelgate and others, 1992). This upwarp was initially thought to be a mud volcano, but deep-towed seismic-reflection data showed internally coherent reflectors, suggesting a structural origin (Cochrane and Lewis, 1988). The upwarp offers much information about the timing and development of the Wecoma fault, and is therefore discussed here in some detail. It is a complex structure that is bounded on the south by the southern strand of the Wecoma fault and on the other three sides by minor reverse faults, but it is best described as a doubly plunging NNW-trending anticline (figs. 7 and 10). The three dimensional structure of the upwarp is shown in the composite block diagram shown in figure 10.

Magnetic modeling of the upwarp and Wecoma fault indicates that basaltic basement is upwarped beneath the fold in the sedimentary section, and is vertically offset approximately 100 meters by the fault, north block up (Appelgate and others, 1992). Based on the involvement of the basement and the right step in the fault, we interpret the upwarp as a restraining-bend anticline formed by compression across the right step in the Wecoma fault (Sylvester, 1988). We hereinafter refer to the upwarp as a pressure ridge (PR). Alternatively, the ridge may be a truncated early-formed anticline of the type described by Wilcox and others (1973). If this model is applicable, the anticline may have formed in the sedimentary section in response to left-lateral displacement of the underlying Juan de Fuca plate, and then was partially truncated by two en-echelon segments of the fault as they propagated upward with increasing fault motion. If this is correct, the lack of a single throughgoing trace implies that the fault has not completed its final stage of development into a throughgoing single strand as modeled in clay experiments and observed in nature (Wilcox and others, 1973). A second alternative explanation is that the upwarp is related to the growth of the accretionary wedge (Cochrane and Lewis, 1988). If this is the case, the ridge would be linked to the master décollement by an undetected basal detachment. However, analysis of the growth history of the ridge, discussed below, indicates that the ridge is roughly twice the age of the marginal ridge, and began its growth when it was 28-32 km west of the longitude of the present deformation front, using the 40 mm/yr Juan de Fuca-North America convergence rate of DeMets and others (1990). The relative longevity of the ridge, and the evidence for a basement upwarp suggest that its formation was unrelated to growth of the frontal thrusts of the accretionary wedge. It is probable, however, that recent growth has been augmented by horizontal compression due to the proximity of the plate boundary.

Age, Net Slip, and Average Slip Rate of the Wecoma Fault

Stratigraphic relationships within the abyssal-plain sedimentary section in the vicinity of the Wecoma fault and the pressure ridge can be used to infer the growth history of the pressure ridge as well as the slip-rate and horizontal separation on the Wecoma Fault.

Abyssal Plain Stratigraphy

We have informally divided the abyssal-plain sedimentary section into four seismic-stratigraphic units on the basis of reflection character and stratigraphic coherence using the 1989 MCS data (fig. 8B). The lowest unit (unit 4) is a weakly reflecting seismic unit that directly overlies the basaltic rocks of oceanic layer 2. The poor reflectivity of this unit is probably due to its lithologic homogeneity, consisting of poorly stratified carbonate oozes, calcareous mudstone, and silt turbidites at DSDP drill site 174 on Astoria Fan (Kulm, von Huene and others, 1973). Thickness of this unit is variable because it fills in the rough basement topography, but it averages approximately 300 m in the vicinity of the pressure ridge. Units 2 and 3 are defined somewhat arbitrarily on the basis of prominent reflectors, and consist primarily of distal thin-bedded silty clay turbidites interbedded with hemipelagic clay (Kulm, von Huene and others, 1973). Units 2 and 3 are an abyssal-plain sequence that is thought to have either a Klamath Mountain or Vancouver Island source (Kulm and Fowler, 1974). Units 2 and 3 both thicken uniformly eastward in response to increasing rates of sedimentation and the eastward slope of the 9-11 Ma crust presently being subducted (Wilson and others, 1984). The uppermost unit (unit 1) is composed of overlapping lobes of the middle to late Pleistocene Astoria Submarine Fan (Kulm, von Huene and others, 1973). The lithology of unit 1 is dominated by thin to thick bedded medium to very fine-grained sand intervals with sharp lower contacts, grading upward into silts and silty clays (Kulm, von Huene and others, 1973). Not visible on figure 8B is a capping fifth unit consisting of 1-2 meters of Holocene hemipelagic silt and clay (Nelson, 1976; this study).

Timing Constraints

Seismic profiles are notoriously poor at resolving stratigraphic and timing relationships in strike-slip fault zones. However, the closely spaced MCS lines near the Wecoma fault, and the fortuitous presence of critical timing indicators have allowed us to bracket the interval in the stratigraphic section at which vertical motion of both the fault and the pressure ridge began. On MCS line 37 (fig. 8B) unit 1 clearly shows thickening of the unit as a whole and of individual acoustic intervals on the downthrown (south) side of the fault, indicating that the Wecoma fault has been active for most of the depositional history of the Astoria Fan. On line 45 (fig. 9), the same units are seen to thin across the pressure ridge, indicating that vertical development of the ridge occurred during the same time interval. Thickness trends in units lower in the section on both lines are unaffected by the presence of the fault, indicating that they pre-date the Wecoma fault. Alternatively, Appelgate and others (1992) have interpreted apparent stratigraphic pinchouts against the pressure ridge as suggesting an early history for the basement upwarp, inferring that ridge formation occurred shortly after the formation of the crust at the spreading ridge (see unit 4 on figure 9). However, the morphology of the basement upwarp from magnetic modeling and MCS profiles matches that of the folded sedimentary section, indicating that folding occurred following deposition of most of the sedimentary section. Additionally, the pinchout of unit 4 is only observed on some reflection profiles of the upwarp, while others clearly show it to be an artifact. We therefore now interpret this apparent pinchout as a superimposed side echo of the upwarped basement on unit 4. OSU MCS line 30 and U.S.G.S. line 77-12, neither of which cross the upwarp, show this superimposed side echo clearly (see fig. 3 for location of these lines).

On close inspection, the division between pre-faulting units and syn-faulting units (reflector "S" on figs. 8B and 9) can be identified at a depth of 4.30 seconds on line 37 (abyssal plain, upthrown side), and 3.82 seconds in line 45 (top of the pressure ridge). Reflector "S" was identified by examining the thickness of each stratigraphic sub-unit on these two lines and picking the reflector that separated units that showed fault related thickness trends from those that did not. Units 2 and 3 show just the reverse thickness relationship, with thinner units on the downthrown side of the fault (fig. 8B). This relationship is maintained along the length of the fault, suggesting that the fault was not active in a vertical sense during unit 2 and 3 deposition, or that the sense of vertical motion was south block up. Since reflectors consistently show a south block down separation, we can attribute these thickness changes across the fault to left-lateral strike-slip displacement of the eastward thickening wedges of sediment (i.e., left slip moves thinner wedges of sediment eastward on south side of fault relative to the north side). Note that not all reflectors need show any vertical separation on seismic profiles of strike-slip faults, and in fact some do not on figure 9 even though other evidence discussed below demonstrates 5-6 km of net slip on the fault. Growth of the pressure ridge anticline appears to have been coeval with slip on the Wecoma fault, since the seismic reflectors in both lines 37 and 45 (reflector "S") that separate pre-faulting and syn-faulting sediments are approximately the same reflector when traced over the intervening distance on a crossing reflection line. The high quality of the data allows correlation over tens of kilometers with a high degree of confidence.

In order to establish the age at which fault motion began, we have correlated a prominent seismic reflector at the base of the Astoria Fan with the same interval drilled at DSDP site 174, 70 km to the southwest of the pressure ridge (figs. 1 and 11). Fortuitously, during the initial survey for site 174, a seismic-reflection profile was made that connects the drill site to the pressure ridge anticline (Kulm and others, 1973, their fig. 2, line A-C). This allows a direct tie between the anticline and the drill site. The change in reflection character above this reflector (fig. 8B; base of unit 1) can also be traced to the drill site. At the drill site, the profound lithologic change between the sand turbidites of the fan and the silt turbidites of the plain sequence was observed at the depth of this reflector in the cores (fig. 11). Matching reflectors with their respective lithologic changes in the cores also allows accurate calculation of seismic interval velocities at the drill site.

Ingle (1973) plotted the coiling directions of the planktonic foraminifer *Globigerina pachyderma* in the cores from site 174 (fig. 12). Notable are three dextral coiling events at depths below the surface of 0-40 m, 125-135 m, and 238-295 m. The lowest of these three events brackets the depth at which the base of the Astoria fan section was encountered in the hole (284 m). Ingle (J. Ingle, Stanford Univ., written comm., 1991) has tied these dextral coiling events to regional northeast Pacific paleooceanographic events, which are dated with magnetostratigraphy and tephrochronology. By this method the upper and lower bounds of the lowest coiling event are dated as 600 ka and 800 ka respectively (fig. 12). Interpolating from these bracketing ages with sedimentation rates, the age of the base of the Astoria fan section at site 174 is 760 ka ± 50 ka, with the error bars reflecting uncertainties in using uniform sedimentation rates and in the precision of determining the age of the coiling events. To estimate the age of this same reflector near the Wecoma fault, we infer that there is no significant time transgression between site 174 and the pressure ridge. We make this inference because no significant onlap or offlap relationships are observed within several hundred meters vertically of the base of the fan (fig. 11); the reflector is nearly horizontal, and the trend of the seismic section is approximately perpendicular to the sediment transport direction. Using an average sedimentation rate of 110 cm/1000 yrs calculated from the age, thickness, and seismic velocity of the fan section at the Wecoma fault, the age of reflector "S", and thus the age of vertical motion on the Wecoma fault, is estimated to be 600 ± 50 ka. Although additional uncertainties exist in sedimentation rates, age correlation of the base of the fan, and seismic velocities, we use the same error bars here because we are unable to quantify them independently.

Fault Restoration

We have taken advantage of the geometry of the abyssal plain units in order to calculate the net-slip on the Wecoma fault. Pre-faulting sedimentary units strike mostly north-south, and thicken uniformly eastward, resulting in eastward thickening sedimentary wedges. Slip on the Wecoma fault has cut and juxtaposed these wedges such that thickness changes across the fault are pronounced. On MCS line 37, units 2 and 3 are thinner on the south (downthrown) side (fig. 8B). We attribute this abrupt thinning across the fault to be the result of left-lateral translation of the eastward thickening wedges comprising these two units (we assume negligible differential loading of these units due to thickness changes in unit 1). In order to estimate the horizontal separation along the Wecoma fault, we have restored the abyssal-plain section by reversing the left-lateral motion on the fault (fig. 13). The blocks were translated *right-laterally* until the eastward thickening wedges of sediment matched. Using this method, the thickness match across the fault was made simultaneously with 18 individual reflectors within units 2 and 3, reducing the error inherent in picking only a few reflectors. The horizontal motion needed to restore the section is 5.5 ± 0.8 km.

We have also plotted isopachs of units 2 and 3 as an alternative method for determining horizontal separation. Figure 14 is the isopach plot of unit 2, following smoothing and removal of a velocity artifact. The isopach plot reveals a pattern of left offsets of individual contours, decreasing northwestward to zero at the fault tip 17-20 km seaward of the deformation front. The offset of the contours near the deformation front is 3.7 ± 0.5 km, determined by averaging the three easternmost contours. We attribute this somewhat different result to poor constraint on the contours south of the fault, and disruption of thickness trends near the adjacent pop-up. Additionally, the isopach offset depends on only three piercing points, whereas the retrodeformation uses 18. We thus infer that the retrodeformation method is the best method of estimating horizontal separation, and we use the value 5.5 ± 0.8 km in the slip-rate calculations below. Neglecting the 100 m of vertical separation, this value represents the net slip on the Wecoma fault near the deformation front.

A potential source of error in the use of time versus thickness is the possibility of lateral velocity changes in the selected units. However, lateral velocity changes, if present, are most likely to be oriented normal to the deformation front, and thus have negligible effect on restoration of the sedimentary section. Unfortunately, the youngest unit (1) cannot be used for an independent estimate of net slip during deposition of the youngest part of the fan section because vertical movement on the Wecoma fault has influenced thickness of this unit.

Using the previously calculated age of the fault and the net slip estimate above, we calculate that the average slip rate of the Wecoma fault since its inception 600 ± 50 ka ago has been 7-10 mm/yr near the present deformation front. These rates depend on the estimated age of the fault, which may include an error bar that is too small as discussed above. Thus the calculated slip rate may have a larger error bar than calculated here.

Late Pleistocene-Holocene Slip Rate

SeaMARC 1A sidescan imagery shows that the Wecoma fault offsets left-laterally a late Pleistocene distributary channel and an older slump scar on the Astoria submarine fan (OC and OS, figs. 6; offset channel, fig. 15). Horizontal separations are about 120 ± 5 m and 350 ±10 m, respectively (Appelgate and others, 1992; this study). These crosscutting relations can be used to obtain an independent estimate of the slip rate during latest Pleistocene and Holocene time. The offset channel, in particular, offers the best opportunity for estimating the Holocene slip rate. The channel is blocked 18 km upstream (to the north) by slump debris from a 32 km^3 slope failure (fig. 4 and 5 labeled slump debris). The slump is apparently a bedding plane slide from the western flank of the leading landward-vergent accretionary thrust ridge. We estimate the age of this slump to be 10-24 ka, based on a ^{14}C date from a gravity core taken from a sediment drape on top of one of the slump blocks and on onlapping relations observed on a high-resolution seismic record. In the reflection profile, the slump debris rests directly on the seafloor reflector with no visible sediment onlap or ponding around the slump blocks. Using a composite late Pleistocene-Holocene sedimentation rate derived from Nelson (1968) and this study, we estimate that sediment accumulation following the slump could not continue for more than about 24 ka without depositing a thick enough unit to be detectable on the MCS profile, thus setting a maximum age for the slump. We derive the minimum age for the slump from the ^{14}C age of sediment at the bottom of the above mentioned core. The core sampled only post-slump hemipelagic sediment, and thus the 10,300 Y.B.P. date from the lowermost part of the core sets the minimum age of the slump at about 10 ka.

Because the fault is older than either the slump or the channel, a slip-rate can be estimated from the channel offset shown in figure 15. The channel wall must have been cut prior to blockage by the slump, establishing the minimum age at about 10 ka (i.e., the minimum age of the slump). Similarly, a maximum age for the channel wall is constrained to be the same as the maximum age of the slump. Channel cutting should have ceased or been greatly reduced following the blockage, thus younger fault motion would offset the channel wall, as presently observed, without modification by erosion. If channel cutting and fault motion were simultaneous, the high frequency of late Pleistocene turbidity currents carrying large quantities of sand and gravel (Duncan 1968; Nelson, 1968; Griggs and others, 1970) should have eroded the offset to something other than the crisp separation seen in sidescan images (fig. 15). Seismic-reflection records showing the truncation of deep sea channel walls (Griggs and Kulm, 1973) and numerous sediment hiatuses in cores from the axial portion of these channels (Griggs and Kulm, 1970) document the erosive character of the coarse-grained late Pleistocene turbidity currents in this region. Given this reasoning, the age of the channel wall is probably 10-24 ka, consistent with incision during the last episode of high turbidity current activity during the latest Pleistocene low-stand of sea level. Using this age range, we calculate a latest Pleistocene-Holocene slip-rate of 5 to 12 mm/yr. These rates are comparable to the 7 to 10 mm/yr average rate calculated from the net horizontal displacement since inception of the fault.

Intersection of Wecoma Fault and the Accretionary Wedge

The complex structure of the area where the Wecoma fault intersects the initial thrust ridge indicates that this fault is not simply overridden by the accretionary prism. High-resolution SeaMARC 1A sidescan records of the intersection zone on the abyssal plain show that this area is dominated by a nested series of uplifted asymmetrical triangular plateaus or pop-ups, bounded by reverse faults (figs. 6, 7, and 16). The single trace of the Wecoma fault separates into several diverging splays at the western tip of the largest of the pop-ups (labeled A on figs. 6, 16, and 17), the largest of these becoming the southern bounding fault of the pop-up. Sidescan and MCS records suggest that the main trace is buried by slump debris along much of its length in this area (Appelgate and others, 1992). The pop-up plateaus appear to be the result of a complex interaction between the strike-slip fault and the evolving deformation front. The model we prefer for their development is shown in figure 17. The plateaus are uplifted between divergent splays of the main strike-slip fault, and possibly driven westward by horizontal compression because of their proximity to the plate boundary. Appelgate and others (1992) suggest that the high vertical scarps between the offset channel and the western tip of the pop-up (fig. 6) are the result of 2.5 km of left-lateral displacement of a part of the pop-up.

Influence of the Wecoma Fault on the Accretionary Wedge

The eastern end of the above described pop-up directly abuts the western flank of the first accretionary ridge of the North American plate (fig. 6, MR). On the west side of the initial thrust ridge, the plate boundary forms an

embayment corresponding to the width of the adjacent pop-up on the abyssal plain (Appelgate and others, 1992). A seaward-vergent thrust segment occupies the area of the embayment in an overall landward-vergent thrust setting described by MacKay and others (1992). This suggests that a local reversal of vergence in the leading accretionary ridge may be related to the effects of the strike-slip fault underthrusting the wedge. The mechanism for this vergence reversal may be a local reduction in pore fluid pressure due to fluid venting by the Wecoma fault. Such a pressure loss would increase the basal shear stress along the decollement, promoting development of the seaward-vergent segment (Tobin and others, 1991). The ridge formed less than about 300 ka based upon microfossil evidence from rocks dredged from the ridge (Carson, 1977). The embayment is bounded by linear gullies that cut upslope into the initial thrust ridge, and other such gullies lie within the embayment (fig. 6). We interpret these linear gullies as fault splays related to slip on the Wecoma fault. Observations and samples from the submersible ALVIN confirm that the linear gullies visible in sidescan records are zones of active oblique faulting. Several dives (fig. 18) showed that bedding is extensively sheared, with multidirectional slickensided surfaces and mullions (fig. 19). Shear planes striking WNW, roughly parallel to the Wecoma fault were observed in these gullies. Linear WNW-trending scarps along the strike of the Wecoma fault are also present on the eastern flank of the initial thrust ridge, the crest of which has a small left-lateral offset (fig. 20B). These lineations follow the Wecoma fault trend and are interpreted as fault scarps because (1) they lack the dendritic drainage pattern commonly observed in nearby erosional gullies, (2) they strike at an angle to the bathymetric contours, and (3) because they originate at the highest point on the marginal ridge. MCS line 29 crosses the area of these scarps, and shows a strong vertical disruption of the marginal ridge that we interpret as the cause of the seafloor scarps.

Rocks collected with ALVIN from the gully sites on the seaward flank of the marginal ridge consist of sheared siltstones, sandstones and pebble to cobble conglomerates (Sample and others, 1991; Tobin and others, 1991) that probably originated on the Astoria fan and were re-cemented with a secondary carbonate cement (Kulm and Suess, 1990). The carbonate cement, derived from fluids venting from the shear zones, bonds the sheared sedimentary fragments into an angular breccia that fills the bottoms of the gullies. Isotopic analyses of these pore-fluid derived carbonate cements show that cements in the fault zone differ significantly from those elsewhere in the young accretionary wedge. Fault zone cements from the Wecoma fault have $\delta^{18}O$ values ranging from -4.27 to -12.66‰ (SMOW) and $\delta^{13}C$ values of -1.12 to -25.01‰ (PDB). Cements from an accretionary-wedge thrust on the second thrust ridge 38 km to the south have $\delta^{18}O$ values of +4.37 to +6.70‰ and $\delta^{13}C$ values of -38.47 to -54.23‰. Sample and others (1991) attribute these isotopic ratios within the Wecoma fault zone to: (1) higher fluid temperatures near the Wecoma fault, perhaps as high as 100° C, and (2) a seawater-dominated carbon reservoir derived from deeply-buried sediments or oceanic crust. In contrast, isotopic ratios from the site distant from the strike-slip faults are best explained by oxygen ratios dominated by ambient seawater, and carbon from an oxidized thermogenic methane source, or from biogenic methane and seawater (Sample and others, 1991).

The evidence from fluid chemistry, sidescan images, and seismic profiles indicates that the leading edge of the accretionary wedge is disrupted and offset by the Wecoma fault. We have studied sidescan images, SeaBeam bathymetry, and seismic profiles of the frontal accretionary wedge in order to determine the extent to which these effects can be observed on the continental slope. In high-resolution SeaMARC sidescan images, a steep WNW-trending scarp is observed to terminate the bathymetric expression of several thrust ridges 8-15 km landward of the deformation front (figs. 7 and 20B, labeled scarp). This scarp is sub-parallel to the Wecoma fault and lies along the projected trend of the fault into the accretionary wedge. Using image enhancement techniques, we observe that, in detail, this scarp has as elements several sub-parallel WNW-trending linear scarps that also parallel the trend of the main scarp and the Wecoma fault. These linear features are clearly fault scarps since they cut across the erosional spurs and gullies of the main escarpment at nearly right angles. The seawardmost synclinal axis of the accretionary wedge lies between the northwest end of this scarp and the fault splays that cut the marginal ridge. Near the center of this basin is a WNW-trending linear feature that also lies on the projection of the Wecoma fault (fig. 20). Eight km southeast of this scarp, and 22 km southeast of the deformation front, the projected trend of the Wecoma fault is crossed by U.S.G.S. line 77-11 (figs. 3 & 21). This reflection record shows a near-vertical disruption located at the western edge of a bathymetric bench near the projected position of the Wecoma fault. A surficial bump or scarp overlies the disruption, which affects the uppermost flat-lying sediments of a broad basin. Reflectors deeper in the section show a sharp dip reversal and loss of coherence. The dip reversal might be resolved as a basin if the line were migrated, but we think it is too abrupt and the radius of curvature of the beds too short for this interpretation, and thus we interpret this feature as a vertical fault, possibly the landward extension of the Wecoma fault.

Having found possible evidence for an upper plate continuation of the Wecoma fault some 10-20 km southeastward into the accretionary wedge, we searched for evidence of termination or continuation of the fault, as well as faults B and C, higher on the continental slope. We used academic, U.S.G.S., N.O.A.A., and industry

seismic-reflection profiles, as well as GLORIA long-range sidescan images and N.O.A.A. SeaBeam high-resolution bathymetry, now available from the abyssal plain landward to approximately the shelf break in northern Oregon.

We observe that several prominent WNW-ESE bathymetric trends cross the continental slope off central Oregon (fig. 5). These trends are composed of NW- to WNW-trending folds and scarps of 5-40 km in length. They appear prominently on the slope because they cross obliquely the N- to NW-trending grain of the accretionary wedge, and because the deformation within these zones is more intense than in the surrounding wedge. In several cases the oblique folds are accretionary-wedge folds whose axes have been sigmoidally bent to the northwest, while others are fault-bend and fault-propagation folds overlying steeply dipping oblique faults. In map view, SeaBeam bathymetry and GLORIA images show left-stepping sigmoidal bending of fold axes along these trends, left offsets of fold axes, and linear WNW-trending scarps (fig. 22). These features were mapped using continuous GLORIA long-range sidescan on the continental slope and continuous SeaBeam bathymetry on the slope and outermost shelf. The deformation of accretionary-wedge structures observed in the perspective SeaBeam mesh plot (fig. 5) and in map view (fig. 22) takes a variety of forms, but older structures are systematically disrupted and younger structures developed along these throughgoing zones to the extent that they are well expressed in the bathymetry.

Three of the WNW-trending slope deformation zones (labeled WF, B, and C on fig. 5) lie adjacent to the Wecoma fault and faults B and C respectively, and have similar trends to the abyssal-plain faults. The zones begin on the middle to lowermost slope and continue southeastward to the shelf break, where bathymetric expression dies out (figs. 4 and 5). At least one oblique deformation zone does not lie on the landward projection of an abyssal-plain fault, although it is structurally and morphologically similar to the other three (see unnamed zone between fault B and the Wecoma fault on fig. 4). The zone marked WF on figure 5 extends southeastward from the area where scarps and offsets related to the Wecoma fault were mapped with sidescan imagery (fig. 20). This deformation zone is crossed by several seismic-reflection lines, including four OSU lines, two U.S.G.S. lines, and two industry lines in our data set. These profiles clearly show the oblique folds observed on the SeaBeam bathymetry, and most also show that the deformation zone includes several major and many minor high-angle faults. Several profiles reveal that the oblique folds that define the bathymetric deformation zone are fault-bend and fault-propagation folds, both landward and seaward vergent, developed above high-angle faults. Detailed mapping suggests that some of these oblique folds are superimposed on somewhat older NW-to NNW-trending folds. Those that overlie high-angle faults show, by their trends, that the underlying faults also trend NW to WNW. In some reflection crossings, the high-angle faults are expressed as a nearly vertical main trace, commonly with attendant flower structures of varying degrees of development (fig. 23C). Development of oblique folds and faults decreases or becomes more distributed southeastward (landward) toward the upper slope and outermost shelf within the deformation zone. We also note the presence of two deformation zones, similar to the others, (fig. 4, located between the Wecoma fault and fault B, and seaward of Tillamook Bay) that do not lie on the projected trends of abyssal-plain faults.

DISCUSSION

Fault Orientation

The Wecoma fault strikes 293° ± 3° on the abyssal plain, the same as the strikes of faults B and C. This orientation is virtually the same as the 295° strike of the Blanco fracture zone, the transform fault that separates the Juan de Fuca and Pacific plates and forms the boundary between the Gorda segment and the main segment of the Juan de Fuca plate (fig. 1). Thus the Wecoma fault, faults B and C, and the Blanco fracture zone are oriented along small circles of rotation of the Juan de Fuca plate with respect to the Pacific plate. It is presently unknown if this orientation is coincidental, or if there is a fundamental relationship between plate motion and the orientation of the strike-slip faults. An attractive explanation for this similarity might be that the strike-slip faults are re-activated minor transforms formerly generated at the spreading ridge that are currently responding to the subduction related stress field at the deformation front. Detailed reconstructions of the spreading history of the Juan de Fuca plate by Wilson and others (1984), however, indicate that the Juan de Fuca ridge was oriented nearly north-south at the time the presently subducting crust was generated. Any relict transforms generated at that time should be oriented east-west, making it unlikely that reactivated faults are responsible for the observed structures. Although the reflection profiles have been interpreted to include the possibility of a long (> 6 Ma) history for the Wecoma fault (Appelgate and others, 1992), our preferred interpretation suggests that the faults are on the order of 600 ka, eliminating a spreading-ridge origin. The youth of these faults, and their proximity to and influence on the plate boundary suggest that they are a subduction-related phenomenon as opposed to relict structures or structures related to regional Juan de Fuca plate stresses. Indeed, limited seismological evidence that suggests the regional stress field may be roughly north-south in much of the Juan de Fuca Plate (Spence, 1989) is incompatible with the orientation and slip direction of the abyssal-plain strike-slip faults.

Strike-Slip Faults and the Accretionary Wedge

We have shown that the Wecoma fault influences the seawardmost accretionary wedge. Seismic and sidescan records show that the intersection of the fault and the deformation front is a complex zone of interaction between the frontal thrust and the strike-slip fault. Strands of the fault extend into the seawardmost three or four thrust ridges on sidescan records, and these observations are supported by direct observation from Alvin and analysis of carbonates derived from venting fluids on the marginal ridge. Detailed mapping of the continental slope off northern and central Oregon has also documented five oblique deformation zones, three of which lie along the landward projections of the three abyssal-plain strike-slip faults (fig. 4).

In addition to seismic reflection and sidescan evidence, we observe that there are significant differences in the style and growth history of the youngest thrust ridges in the vicinity of the Wecoma fault. Considerably more shortening has occurred on equivalent structures immediately south of the projection of the Wecoma fault than to the north. Both fault-bend folds, and fault-propagation folds are better developed to the south, and an additional thrust ridge is present to the south that is not present to the north (fig. 24). This change in fold and thrust development across the Wecoma fault is clear on reflection profiles, and can also be seen in the bathymetry, which shows an abrupt bathymetric change across the fault (fig. 24; see also MacKay and others, 1992). The bathymetric change corresponds to the scarp discussed above and shown in figure 20. Much of the bathymetric change is due to the abrupt increase in development of the thrusts on the south side.

The structure map of this area (fig. 7) shows that other changes in accretionary-wedge structures also occur along this bathymetric trend and escarpment (labeled scarp on Figure 7). Some fold axes and thrust faults step or bend to the left, while others terminate altogether. Similar relationships between trench-parallel accretionary-wedge structures and a conjugate set of strike-slip faults have been mapped in the Shumagin segment of the Aleutian forearc (Lewis and others, 1988). The projected trend of the Wecoma fault also coincides with an abrupt change in strike of the seaward thrust ridges. North of the fault they strike approximately north-south; south of the fault, the strike is 340°. The left offsets and sigmoidal bending are consistent with a left-lateral shear zone. The differences in thrust development across the projection of the Wecoma fault also support the presence of an active left-lateral shear zone. Given the convergence rate of 40 mm/yr (DeMets and others, 1990) and a simple calculation of the shortening on these structures, we estimate that the four westernmost thrusts must have formed during the 600 $\pm$ 50 ka the Wecoma fault has been active. We postulate that the difference in shortening is due to a local change in the subduction rate across the fault resulting from subduction of the active Wecoma fault. Using the net slip of 5.5 $\pm$ 0.8 km and the 600 $\pm$ 50 ka age of the Wecoma fault, the difference in subduction across the fault has been 8.4-10.0 km, or 41-44% of the 19-24 km of normal convergence that has occurred during the life span of the Wecoma fault. Figure 25 illustrates this geometric result, and shows that the effective local convergence rate is 28% greater south of the Wecoma fault than to the north. We postulate that increased convergence south of the Wecoma fault due to this difference has caused the extra shortening in the seaward thrust ridges, and probably also the early development of the 'extra' thrust.

Implications for Cascadia Convergence

We suggest three hypotheses to explain the possible interactions of the abyssal-plain faults and the accretionary wedge: 1) The strike-slip faults extend from the abyssal plain beneath the accretionary wedge and are the source of the deformation zones; 2) The strike-slip faults originate within the North American Plate, and propagate into the subjacent subducted slab and seaward into the abyssal plain; and 3) The deformation zones on the slope are unrelated to the abyssal-plain faults.

If the strike-slip faults originate in the Juan de Fuca Plate (hypothesis 1), the deformation zones in the accretionary wedge may have developed in response to strike-slip motion of the "basement" beneath the accretionary wedge and thick Tertiary shelf sequence (Sylvester, 1988; Wilcox and others, 1973). If this is the case, the presence of such deformation in both the overriding and downgoing plates presents a problem in reconciling strike-slip motion and oblique convergence over the last 600 ka. Oblique convergence of approximately 24 km directed N62°E has occurred over the past 600 ka, using the plate vectors of DeMets and others (1990). During that time, the points at which the three strike-slip faults on the abyssal plain intersect the present deformation front should have moved some 20 km to the north (neglecting the unknown amount of advance of the deformation front), yet we observe little or no offset between the abyssal plain and accretionary-wedge segments of these faults. The discrepancy could be due to a very recent cessation or slowdown of subduction. Although cessation is unlikely given preponderance of geologic and geophysical evidence, a significant slowdown cannot be ruled out, and could reduce the missing component of convergence (Riddihough, 1984). Three structural explanations might also be considered: (1) Right-lateral strike-slip fault(s) in the upper plate to the east of the youngest accretionary thrusts. Such faults can decouple the seaward part of the accretionary complex and accommodate the margin-parallel component of oblique convergence

(Fitch, 1972; Jarrard, 1986; Karig and others, 1986). Snavely (1987) has mapped such a fault (the Fulmar fault) on the Oregon shelf. More than 200 km of dextral slip occurred on this fault, primarily in the Eocene, but minor offsets of younger units may indicate continued or renewed activity (Snavely, 1987; Snavely and others, 1985). (2) A right-lateral component on the thrusts themselves could accommodate the missing north-south convergence component, distributing the expected offset of the strike-slip faults over many crossing structures. The deformation zones on the slope do show a tendency to step or bend to the south, a requirement of this mechanism; or (3) The subducted strike-slip faults leave progressive deformation behind in the upper plate as they pass beneath it to the northeast. The oblique deformation zone limited to the accretionary wedge between the Wecoma fault and fault B might represent deformation localized at a former position of the Wecoma fault (see fig. 4). This might be analogous to the trail of volcanoes left on a lithospheric plate as it passes over a fixed mantle hot-spot. As the Juan de Fuca plate is subducted, lower plate-faults leave behind a "trail" of deformation in the accretionary wedge as they pass obliquely beneath the North American plate.

If the strike-slip faults originate within the upper plate (hypothesis 2), several problems with hypothesis 1 are avoided. Since not all the mapped deformation zones on the slope have abyssal-plain counterparts, an upper-plate origin does not require a separate explanation for those structures. It is also more mechanically reasonable to envision faults in the thicker upper plate propagating across a locked interface into the thin, relatively warm subducting plate than the reverse. The apparent incompatibility of WNW-trending left-lateral faults with the focal solutions and inferred north-south principal stress of Spence (1989) for the Juan de Fuca Plate can be resolved if the abyssal-plain faults are only the western extensions of faults that originate within the upper plate to the east. If this is the case, the regional stress field in the oceanic plate might coexist with a somwhat different stress field within the upper plate and in the vicinity of the deformation front, with a transition somewhere seaward of the abyssal-plain faults. Lastly, a domain of sub-parallel left-lateral strike-slip faults should rotate clockwise through time (Freund, 1974; Ron and others, 1984; Scotti and others, 1991). Such rotations as a result of progressive slip on these faults are suggested by Goldfinger and others (1992), and could resolve the question of offset across the deformation front expected in hypothesis 1, since clockwise rotation of the upper plate could make up the missing north-south component of plate convergence.

Hypothesis 3, that there is no connection between the slope deformation zones and the abyssal-plain faults, must be considered since data positively linking these structures is not available at present. However, the trends, shear sense, and youth of these structures all strongly suggest at least a genetic connection, if not a physical one. If these structures are not directly linked, they may be separate but similar responses by the respective plates to interplate subduction stresses.

CONCLUSIONS

Three WNW-trending left-lateral strike-slip faults in the Cascadia subduction zone offset both the oceanic basement and sedimentary cover of the Juan de Fuca plate. The Wecoma fault, the largest of the three faults, has a measured net-slip of 5 to 6 km at the plate boundary, dying out in the Juan de Fuca plate 18 km to the northwest of its intersection with the deformation front. Two independent estimates of the slip-rate on this fault during two time periods show similar rates of 5 to 12 mm/yr for the most recent 24 to 10 ka period, and 7 to 12 mm/yr over the 600 ka life span of the fault. The Wecoma fault intersects the deformation front in a complex area of structural pop-ups and an embayment in the deformation front. Sidescan images show that scarps and linear gullies extend along the projected strike of the subducted Wecoma fault about 15 km into the accretionary wedge. Slip on the Wecoma fault beneath the North American plate has influenced the development of the initial thrust ridges in the accretionary wedge. Three deformation zones in the accretionary wedge lie along the landward projections of the three abyssal-plain faults. These zones are composed of WNW-to NW-trending folds, sigmoidally bent fold axes, and WNW-trending linear scarps. The style of deformation in these zones is consistent with left-lateral shear zones superimposed on the structural grain of the accretionary wedge. We postulate that these deformation zones are the result of subduction of the active strike-slip faults, or alternatively, that the shear zones originate in the upper plate and propagate across the plate boundary into the Juan de Fuca Plate. The orientation of the Wecoma fault, and the other strike-slip faults along small circles of rotation of the Juan de Fuca/Pacific plate system, is not yet understood.

ACKNOWLEDGMENTS

We thank Richard Perry and Steven Mutula, National Oceanic and Atmospheric Administration, National Ocean Survey, Rockville, MD for preliminary copies of the SeaBeam bathymetry of the Oregon margin. They also allowed us to publish a portion of a 3-D mesh diagram of the northern and central Oregon margin generated at their facility. We thank Sigmund Snelson and Dan Worrall of Shell for the loan of seismic lines on the Oregon and Washington shelf, and for their efforts in locating these lines in the company archives. We also thank Parke Snavely, Sam Clarke, and Dan Orange for thorough reviews of the manuscript. The first two reviewers do not

necessarily agree with all of our interpretations of oblique faults and folds on the upper continental slope or shelf, which are solely our responsibility. This research was supported by NSF grants OCE-8812731 (OSU) and OCE-8821577 (UH) and by the National Earthquake Hazards Reduction Program, U.S. Geological Survey, Department of Interior, under award 14-08-001-G1800 (OSU). Our thanks go to the crews of the vessels R.V. Wecoma, Digicon M.V. Geotide, and R.V. Atlantis II and to Margaret Mumford for drafting the many illustrations.

REFERENCES

Adams, J., 1990, Paleoseismicity of the Cascadia subduction zone: evidence from turbidites off the Oregon-Washington margin: Tectonics, v. 9, p. 569-583.

Ando, Masataka, and Balazs, E.I., 1979, Geodetic evidence for aseismic subduction of the Juan de Fuca plate: Journal of Geophysical Research, v. 84, p. 3023-3027.

Appelgate, T. B., 1988, Tectonic and volcanic structures of the southern flank of Axial volcano, Juan de Fuca Ridge: results from a SeaMARC 1 sidescan sonar survey [M.S. Thesis]: Oregon State University, Corvallis, OR, 161 p.

Appelgate, T. B., Goldfinger, C., MacKay, M. E., Kulm, L. D., Fox, C. G., Embley, R. W., and Meis, P. J., 1992, A left-lateral strike-slip fault seaward of the central Oregon convergent margin: Tectonics, [in press].

Atwater, B. F., 1987, Evidence for great Holocene earthquakes along the outer coast of Washington State: Science, v. 236, p. 942-944.

Atwater, B. F., and Yamaguchi, D. K., 1991, Sudden, probably coseismic submergence of Holocene trees and grass in coastal Washington State: Geology, v. 19, p. 706-709.

Carson, B., 1977, Tectonically induced deformation of deep-sea sediments off Washington and northern Oregon: Marine Geology, v. 24, p. 289-307.

Carver, G.A., Vick, G.S., and Burke, R.M., 1989, Late Holocene Paleoseismicity of the Gorda segment of the Cascadia subduction zone: Geological Society of America, Abstracts with Programs v. 21 no. 5, p. 64.

Clarke, S.H., Jr., and Carver, G.A., 1989, Late Cenozoic structure and seismic potential of the southern Cascadia subduction zone: EOS, Transactions of the American Geophysical Union, v. 70, no. 43, p. 1331-1332.

Cochrane, G. R., and Lewis, B. T. R., 1988, Deep-tow seismic reflection records from the Oregon lower slope: EOS, v. 69, p. 1442-1443.

Darienzo, M. E., and Peterson, C. D., 1990, Episodic tectonic subsidence of late Holocene salt marshes, northern Oregon central Cascadia margin: Tectonics, v. 9, p. 1-22.

DeMets, C., Gordon, R. G., Argus, D. F., and Stein, S., 1990, Current plate motions: Geophysical Journal International, v. 101, p. 425-478.

Duncan, J. R., 1968, Late Pleistocene and postglacial sedimentation and stratigraphy of deep-sea environments off Oregon [Ph.D. Thesis]: Oregon State University, Corvallis, OR, 222 p.

Fitch, T. J., 1972, Plate convergence, transcurrent faults, and internal deformation adjacent to southeast Asia and the western Pacific: Journal of Geophysical Research, v. 77, p. 4432-4460.

Freund, R., 1974, Kinematics of transform and transcurrent faults: Tectonophysics, v. 21, p. 93-134.

Geist, E.L., Childs, J.R.and Scholl, D.R., 1988, The origin of summit basins of the Aleutian Ridge: Implications for block rotation of an arc massif: Tectonics, v. 7, p. 327-341.

Goldfinger, Chris, Kulm, L.D., Yeats, R.S., Appelgate, T.B., Mackay, M.E., and Moore, G.F., 1992, Transverse structural trends along the Oregon convergent margin: implications for Cascadia earthquake potential: Geology, v. 20, p. 141-144.

Griggs, G. B., and Kulm, L. D., 1970, Sedimentation in Cascadia deep-sea channel: Geological Society of America Bulletin, v. 81, p. 1361-1384.

Griggs, G. B., and Kulm, L. D., 1973, Origin and development of Cascadia deep-sea channel: Journal of Geophysical Research, v. 78, p. 6325-6339.

Griggs, G. B., Kulm, L. D., Waters, A. C., and Fowler, G. A., 1970, Deep-sea gravel from Cascadia Channel: The Journal of Geology, v. 78, p. 611-619.

Harding, T.P., 1985, Seismic characteristics and identification of negative flower structures, positive flower structures, and positive structural inversion: American Association of Petroleum Geologists Bulletin, v. 69, p. 582-600

Heaton, T. H., and Kanamori, H., 1984, Seismic potential associated with subduction in the northwestern United States: Bulletin of the Seismological Society of America, v. 74, p. 993-941.

Ingle, J. C., 1973, Neogene foraminifera from the northeastern Pacific ocean, Leg 18, Deep Sea Drilling Project: Initial Reports of the Deep Sea Drilling Project, v. XVIII, p. 517-567.

Jarrard, R. D., 1986, Terrane motion by strike-slip faulting of forearc slivers: Geology, v. 14, p. 780-783.

Karig, D. E., Sarewitz, D. R., and Haeck, G. D., 1986, Role of strike-slip faulting in the evolution of allochthonous terranes in the Philippines: Geology, v. 14, p. 852-855.

Kulm, L. D., and Fowler, G. A., 1974, Oregon continental margin structure and stratigraphy: a test of the imbricate thrust model, *in* Burke, C. A., and Drake, C. L., eds., The geology of continental margins: New York, Springer-Verlag, p. 261-284.

Kulm, L. D., Prince, R. A., and Snavely, P. D., Jr., 1973, Site survey of the northern Oregon continental margin and Astoria Fan: Initial Reports of the Deep Sea Drilling Project, v. XVIII, p. 979-987.

Kulm, L. D., and Suess, E., 1990, The relation of carbonate deposits to fluid venting processes: Oregon accretionary prism: Journal of Geophysical Research, v. 95, p. 8899-8915.

Kulm, L. D., von Huene, R., and the shipboard scientific party, 1973, Initial Reports of the Deep Sea Drilling Project: v. XVIII, p. 97-168.

Lewis, S. D., Ladd, J.W., and Bruns, T.R., 1988, Structural development of an accretionary prism by thrust and strike-slip faulting: Shumagin region, Aleutian Trench: Geological Society of America Bulletin, v. 100, p. 767-782.

Ludwin, R. S., Weaver, C. S., and Crosson, R.S., 1992, Seismicity of Washington and Oregon, *in* Slemmons, D. B., Engdahl, E. R., Blackwell, D., and Schwartz, D., eds., Neotectonics of North America: DNAG CSMV-1, [in press].

MacKay, M. E., Moore, G. F., Cochrane, G. R., Moore, J. C., and Kulm, L. D., 1992, Landward vergence, oblique structural trends, and tectonic segmentation in the Oregon margin accretionary prism: Earth and Planetary Science Letters, [in press].

Nelson, C. H., 1976, Late Pleistocene and Holocene depositional trends, processes and history of Astoria Deep-sea Fan: Marine Geology, v. 20, p. 129-173.

Nelson, C. H., 1968, Marine geology of Astoria deep-sea fan: [Ph.D. Thesis], Oregon State University, Corvallis, OR, 287 p.

Riddihough, R., 1984, Recent movements of the Juan de Fuca Plate system: Journal of Geophysical Research, v. 89, p. 6980-6994.

Ron, H., Freund, R., Garfunkel, Z., and Nur, A., 1984, Block rotation by strike-slip faulting: structural and paleomagnetic evidence: Journal of Geophysical Research, v. 89, p. 6256-6270.

Sample, J. C., Reid, M. R., and Moore, J. C., 1991, Isotopic evidence for deep fluids at the frontal region of the Oregon accretionary wedge: Results from 1990 ALVIN dives, *in* Taira, A., Byrne, T., and Hibbard, J., eds., Muroto Conference on Accretionary Prisms, Muroto City, Japan, May 1991, p. 0-15.

Scotti, O., Nur, A., Estevez, R., 1991, Distributed deformation and block rotation in 3D: Journal of Geophysical Research, v. 96, p. 12,225-12,243.

Snavely, P. D., Jr., 1987, Tertiary geologic framework, neotectonics, and petroleum potential of the Oregon-Washington continental margin, *in* Scholl, D. W., Grantz, A., and Vedder, J. G., eds., Geology and resource potential of the continental margin of western North America and adjacent ocean basins-Beaufort Sea to Baja California: Circum-Pacific Council for Energy and Mineral Resources, Houston, p. 305-335.

Snavely, P.D., Jr., and McClellan, P.H., 1987, Seismic data collected in June, 1976 off the Washington /Oregon coast: U.S. Geological Survey Open-File Report 87-607.

Snavely, P. D., Jr.,Wagner, H. C., and Lander, D. L., 1985, Land-sea geologic cross section of the southern Oregon continental margin: U.S. Geological Survey Miscellaneous Investigations Series Map-1463, scale 1: 125,000.

Spence, W, 1989, Stress origins and earthquake potential in Cascadia, Journal of Geophysical Research, v. 94, p. 3076-3088.

Sykes, L.R., 1989, Great earthquakes of 1855 and 1931 in New Zealand--Evidence for seismic slip along downgoing plate boundary and implications for seismic potential of Cascadia subduction zone: EOS, Transactions of the American Geophysical Union, v. 70, no. 43, p. 1331.

Sylvester, A. G., 1988, Strike-slip faults: Geological Society of America Bulletin, v. 100, p. 1666-1703.

Tobin, H. J., Moore, J. C., MacKay, M. E., Moore, G. F., and Orange, D. L., 1991, Alvin observations at the central Oregon accretionary prism: evidence for fault control of fluid seepage: Geological Society of America Abstracts with Programs, v. 23, p. 103.

Vick, G.S., 1988, Late Holocene paleoseismicity and relative sea level changes of the Mad River slough, northern Humboldt Bay, California: [M.S. Thesis], Humboldt State University, Dept. of Geology, Arcata, CA, 87 p.

West, D.O., and McCrumb, D.R., 1988, Coastline uplift in Oregon and Washington and the nature of Cascadia subduction zone tectonics: Geology, v. 16, p. 169-172.

Wilcox, R. E., Harding, T. P., and Seely, D. R., 1973, Basic wrench tectonics: American Association of Petroleum Geologists Bulletin, v. 57, p. 74-96.

Wilson, D. S., Hey, R. N., and Nishimura, C., 1984, Propagation as a mechanism of reorientation of the Juan de Fuca Ridge: Journal of Geophysical Research, v. 89, p. 9215-9225.

FIGURE CAPTIONS

Figure 1. Plate tectonic configuration of the Juan de Fuca-North American convergence zone. Convergence boundary (dashed heavy line), study area (lined box), abyssal plain drill site 174, and Blanco Fracture Zone (BFZ) are shown.

Figure 2. Trackline map showing the location of all seismic reflection profiles used in this study. Heavy Line DF = Deformation Front (convergence boundary).

Figure 3. Seismic-reflection trackline map and bathymetry in the detailed study area. Depths in meters. Numbered lines are referred to in text.

Figure 4. Generalized structure map of the northern and central Oregon margin. This map emphasizes active features; most structures shown cut or deform the sea floor. The deformation front is a thrust fault south of Fault B, and the base of a seaward dipping ramp north of Fault B. Offsets shown only where demonstrated. No offset across faults may indicate 1) Insufficient data, 2) No horizontal separation, or 3) Horizontal separation not visible at this scale. LV = landward vergence. SV = seaward vergence. SB = slope break. See text and legend for explanation. Modified from Goldfinger and others, 1992.

Figure 5. Perspective fishnet plot of SeaBeam swath bathymetry off central and northern Oregon. View from the southwest showing the physiography of the abyssal plain and accretionary wedge in the vicinity of the Wecoma fault and faults B and C. See text for detailed discussion of features and figure 4 for location of faults. Symbols: BSC = base-of-slope channel; PR = pressure ridge; PU = pop-up plateau; SD = slump debris; and WF = Wecoma fault. B = fault B; C = fault C; CH = Cascade Head on the Oregon coast. Diagram provided by N.O.A.A./N.O.S.

Figure 6. Mosaic of SeaMARC 1A 5 kilometer swaths in the vicinity of the Wecoma fault. Visible are the pressure ridge (PR), the Wecoma fault (WF), the pop-up structure (PU) that marks the intersection of the Wecoma fault with the deformation front (DF); offset channel (OC); offset slump scar (OS); and fault splays (S) that occupy gullies on the seaward flank of the marginal ridge (MR). Embayment in the deformation front (discussed in text) is just east of the pop-up (PU). Location of MCS lines 37 and 45 are shown (solid line).

Figure 7. Structure map of the western portion of the Wecoma fault and frontal accretionary wedge. Structure compiled from migrated and unmigrated seismic reflection profiles, SeaBeam bathymetry, and SeaMARC 1A sidescan imagery. Point "A" corresponds to point A in Figure 17. WF = Wecoma fault; PU = pop-up; PR = pressure ridge anticline; MR = westernmost marginal ridge of the accretionary wedge; OC = offset channel; OS = offset slump scar; DF = deformation front.; ET = the extra thrust referred to in the text; CH = channels. Structures shown as offset only where demonstrated.

Figure 8. A) Migrated MCS line 37 crossing of the Wecoma fault between the pressure ridge and the deformation front (see figures 3 and 6 for location and text for unit descriptions). B) Interpretation of line 37. Note thickening of unit 1 and thinning of units 2 and 3 on the downthrown block. OC = oceanic crust. T = block moving toward the viewer; A = block moving away from viewer. See text for discussion.

Figure 9. Migrated MCS line 45 crossing of the Wecoma fault and the pressure ridge anticline (see Figure 3 for location). Reflector "S" marks the stratigraphic point in the section above which seismic stratigraphic units thin over the ridge crest. Below "S" the stratigraphy does not show the influence of the ridge. This profile crossed the fault just east of the eastern terminus of the Wecoma fault northern strand. See text for discussion.

Figure 10. Composite block diagram of the pressure ridge area and intersection between the Wecoma fault and the deformation front as viewed from the southwest. Migrated seismic sections (two-way time) shown with selected reflectors enhanced. AP = abyssal plain section; AF = Astoria Fan (note thickening across the fault and thinning over the pressure ridge); A = away ; T = toward ; SV = seaward vergence; LV = landward vergence; OC = oceanic crust.

Figure 11. Line drawing of a single-channel reflection profile (OSU cruise YALOC 70, Leg 5) linking DSDP drill site 174A to the pressure ridge anticline and the Wecoma fault. Heavy line marks the base of the Astoria submarine fan at DSDP site 174, and is dated by micropaleontology at 760 ± 50 ka. Inset: Trackline map showing location of seismic profile linking drill site with pressure ridge. See text for discussion.

Figure 12. Lithology and coiling directions of *Globigerina pachyderma* in cores from DSDP site 174. Lowermost dextral coiling event is dated by tephrochronology. Modified from figure 4 of Ingle (1973).

Figure 13. Cartoon illustrating the method used in fault reconstruction. Fault motion was reversed until eastward-thickening sediment wedges of units 2 and 3 matched, resulting in a horizontal separation of 5.5 ± 0.8 km.

Figure 14. Isopach plot of abyssal plain unit 2 (in two way time; see Figure 8A for unit designations). Note westward decreasing left offset of contours by the Wecoma fault. Average offset of 0.625, 0.600, and 0.575 contours is about 4 km. Solid dots are control points.

Figure 15. High-resolution SeaMARC 1A sidescan image of Wecoma fault offsetting the west bank of a late Pleistocene distributary channel on the southeastern Astoria submarine fan. Horizontal separation is 120 ± 10 meters. Light tones represent high backscatter, insonification is from the south. Vertical scarps are the result of strike-slip juxtaposition of irregular sea-floor. Minor faults that also offset the channel wall are interpreted as part of surface expression of flower structure shown in figure 10.

Figure 16. Structural interpretation of the intersection zone and pop-up structure at the intersection of the Wecoma fault and the deformation front. See text for discussion.

Figure 17. Block diagram illustrating structure of the pop-up. Blocks within the flower structure of the Wecoma fault are forced upward and westward by increasing horizontal compression as subduction progresses. Point A corresponds to point A on Figure 6. Adapted from Sylvester (1988, his figure 22 C).

Figure 18. ALVIN submersible tracklines (dive nos. in bold) in the vicinity of the intersection of the Wecoma fault and the deformation front (DF). Several dives focused on the gullies visible on the SeaBeam bathymetry and SeaMARC-1A sidescan images (see also Figure 6). PU = pop-up; Ticks face downslope. See text for discussion.

Figure 19. A and B. Sandy siltstone samples collected with ALVIN from one of the fault-occupied gullies on the seaward flank of the first accretionary ridge. Note slickensided surfaces and mullions.

Figure 20. A) SeaMARC 1A sidescan image of the Wecoma fault crossing the accretionary wedge. Wecoma fault splays cutting the eastern flank of the first accretionary ridge are dimly visible at upper left. At lower right, the linear scarp marking the surface position of the fault is clearly visible. B) Interpretation showing offset of anticlinal axis (marginal ridge) mapped from screen display of sidescan image, which proved to have better resolution than hard copies. Smaller offset by a right-lateral fault shown at lower left (see also inset box on Figure 24 for location of image).

Figure 21. Top: Unmigrated 24-channel seismic profile of the Wecoma fault on the lower continental slope, 26 km landward of the deformation front. Note near-vertical trace, the sharp dip reversals across the fault, and the surface expression. Bottom: Interpreted profile. V.E. = 2.7: 1. See Figure 23 A and Figure 7 for location. (U.S.G.S. Open-File Report 87-607, Snavely and McClellan [1987], their line 77-11).

Figure 22. SeaBeam bathymetry and structure of a portion of the central continental slope traversed by the Wecoma fault (WF). Sigmoidal pattern and offset of fold axes indicative of left-lateral offset on the Wecoma fault. Location of Shell line 7380 (Fig. 23 B) shown by patterned line. For regional location reference, this figure is located at the middle of three "WF" labels on figure 5.

Figure 23. A) Location map of seismic profiles (Figures 21 and 23 B-C).

Figure 23. B) Line drawing of part of Shell line 7380. This single-channel sparker record crosses the Wecoma deformation zone and shows a NW-trending anticline and a truncated syncline separated by a high-angle fault. The anticline is typical of young oblique structures in the deformation zone.

Figure 23. C) Top: Unmigrated single-channel seismic profile of a strike-slip fault within the Wecoma deformation zone on the upper continental slope. Bottom: Interpreted profile. Note near-vertical fault and sharp dip reversals. Oregon State University line SP-56. V.E. = 2.0: 1. See Figure 23 A for location.

Figure 24. SeaBeam bathymetry perspective view along the strike of the Wecoma fault as it crosses from the abyssal plain into the accretionary wedge. Grid spacing is 250 meters. Note the morphologic change in the thrust ridges from the south block to the north block of the Wecoma fault. Note also the "extra" thrust present on the south block with no correlative to the north. Lined box is location of Figure 20. Symbols: PR = pressure ridge; PU = pop-up; DF = deformation front; and WF = Wecoma fault. See text for discussion.

Figure 25. Vector diagram of the inferred local effect of Wecoma fault slip on the plate convergence vector. A) The regional JDF-NAM vector of DeMets and others, 1990. B) JDF-NAM vector (dashed) on the north block of the Wecoma fault. Small arrow is the local vector due to motion of the Wecoma fault. New resultant and convergence rate shown in bold. C) JDF-NAM vector (dashed) on the south block of the Wecoma fault. Small arrow is the local vector due to motion of the fault. New resultant and convergence rate shown with bold arrow. Increased convergence south of the fault may be responsible for the greater shortening and topographic expression of the thrusts south of the Wecoma fault. Calculated from the Euler pole of DeMets et al., 1990, North America fixed.

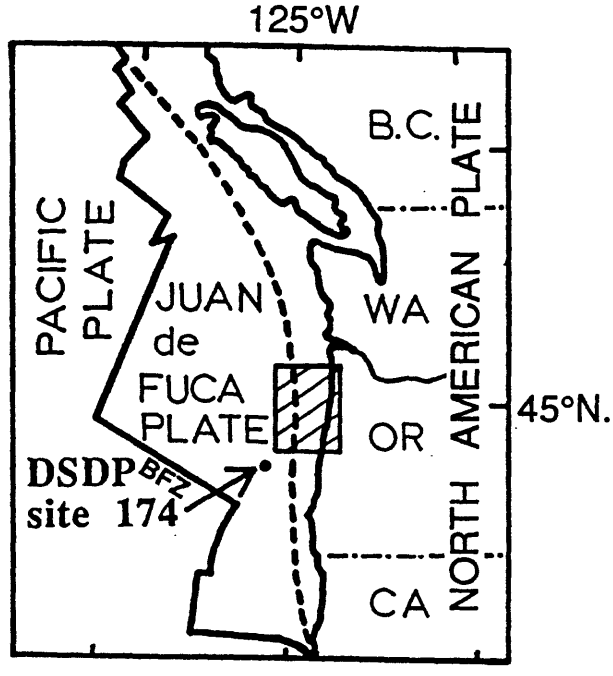
125°W
B.C.
PACIFIC PLATE
JUAN de FUCA PLATE
WA
OR
CA
NORTH AMERICAN PLATE
45°N.
DSDP site 174
BFZ

Figure 1

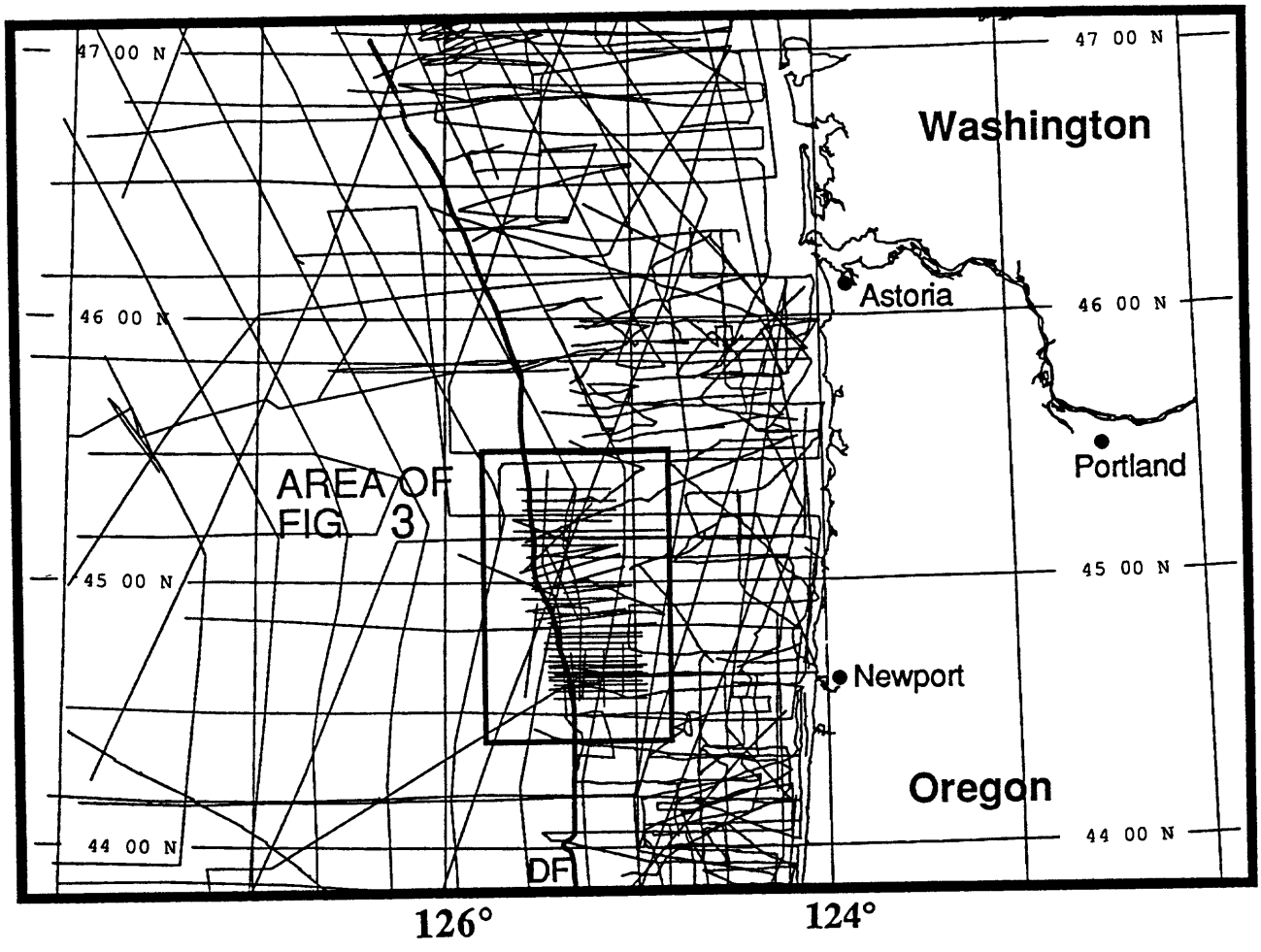
47 00 N
46 00 N
45 00 N
44 00 N
Washington
Astoria
Portland
Newport
Oregon
AREA OF
FIG. 3
DF
126°
124°

Figure 2

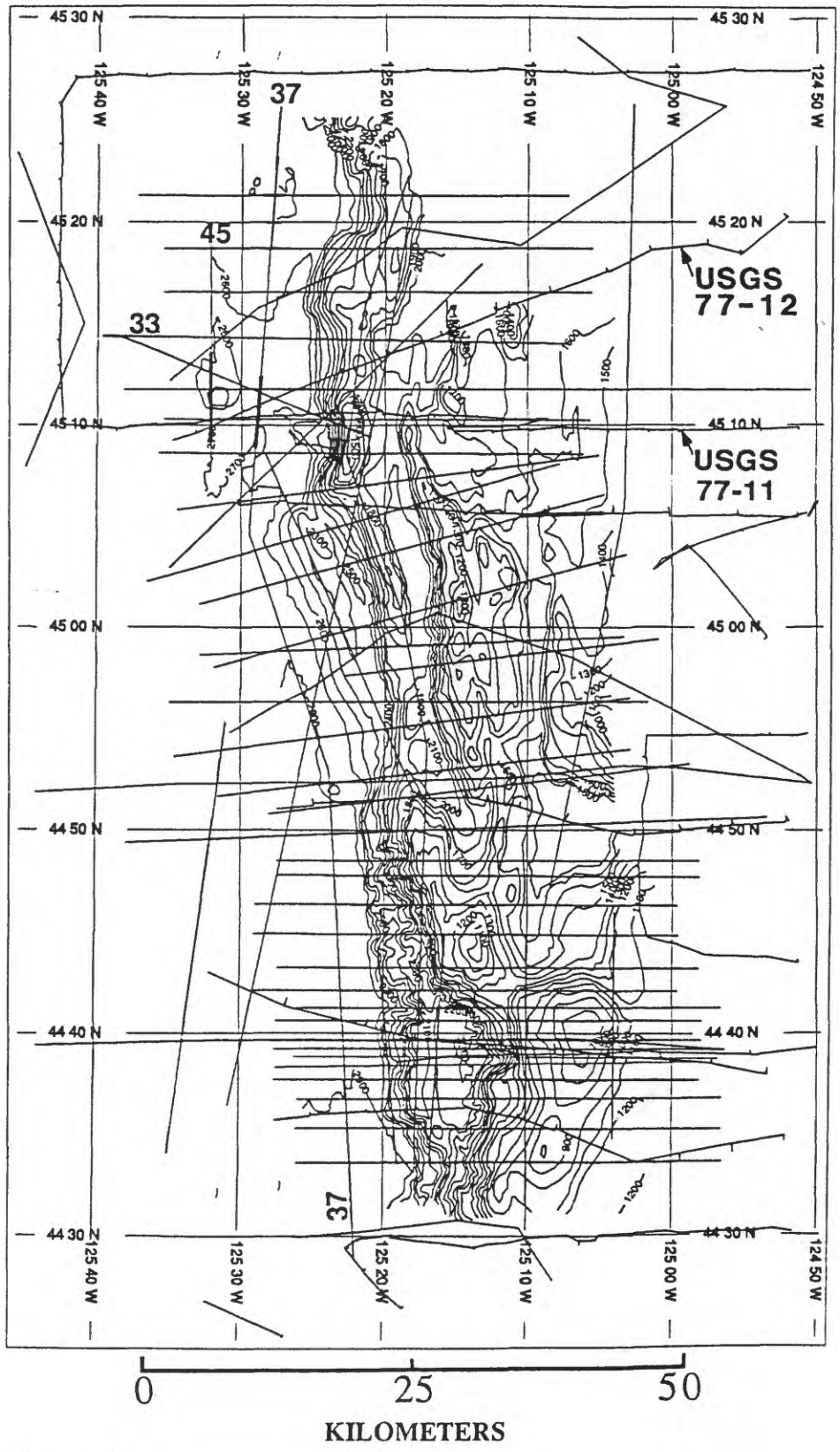
45 30 N
125 40 W
125 30 W
125 20 W
125 10 W
125 00 W
124 50 W
45 20 N
45 10 N
45 00 N
44 50 N
44 40 N
44 30 N
37
45
33
USGS
77-12
USGS
77-11
37
0
25
50
KILOMETERS

Figure 3

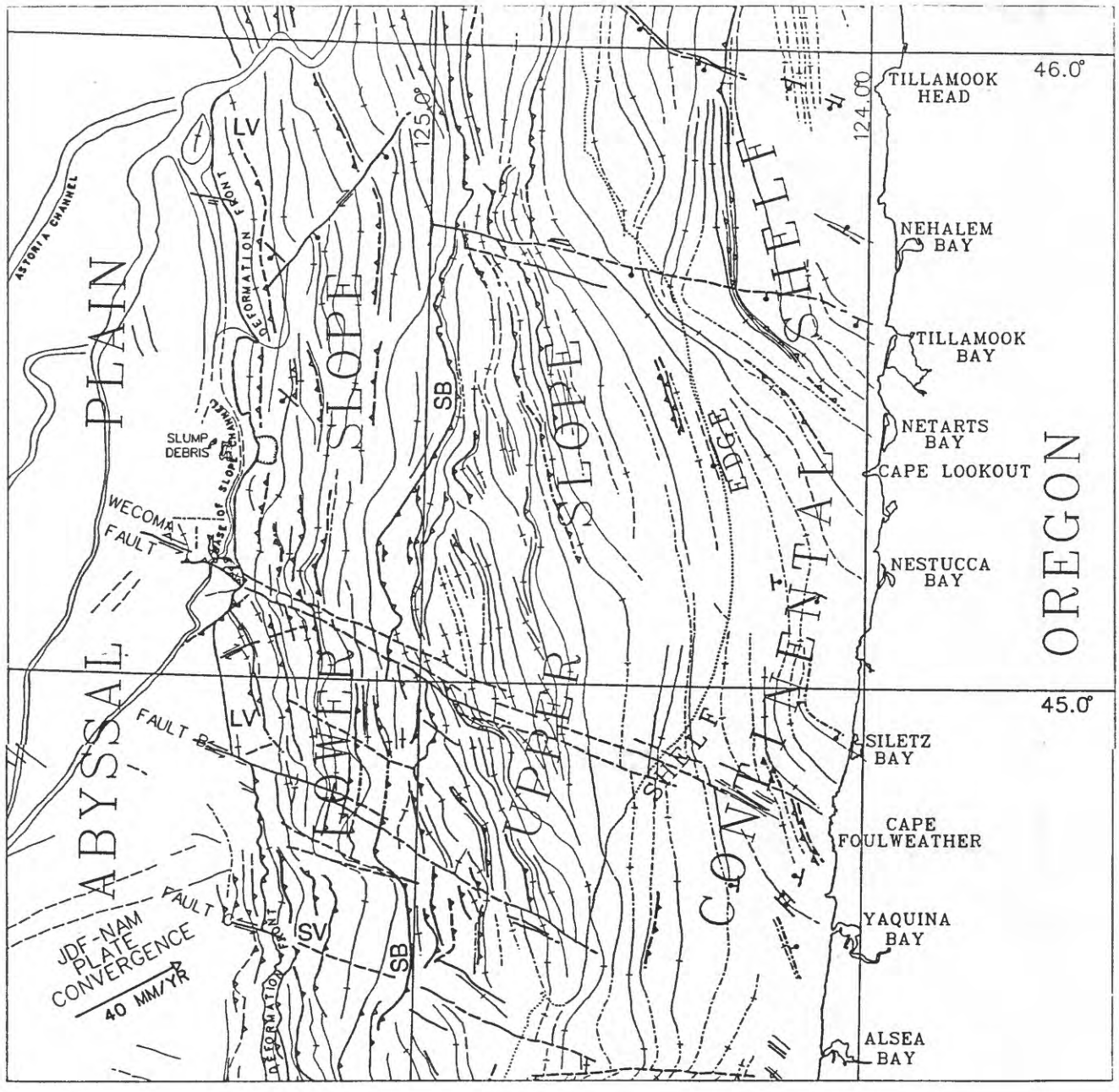

Fault, bar and ball on downthrown side. Arrows indicate relative motion. Dashed where inferred, dotted where concealed.

Thrust fault, sawteeth on upper plate.

Anticline

Syncline

Figure 4

DEPTH (KM)
1
2
3
CH
shelf break
B
B
B
B
WF
WF
WF
C
C
FAULT
ABYSSAL PLAIN
FAULT B
BSC
WECOMA FAULT
PU
PR
SD
ACCRETIONARY WEDGE
125°00'
126°00'
44°30'
44°45'
NORTH
VIEWING ANGLE = 225°
ELEVATION ANGLE = 35°
V.E. = 6:1

Figure 5

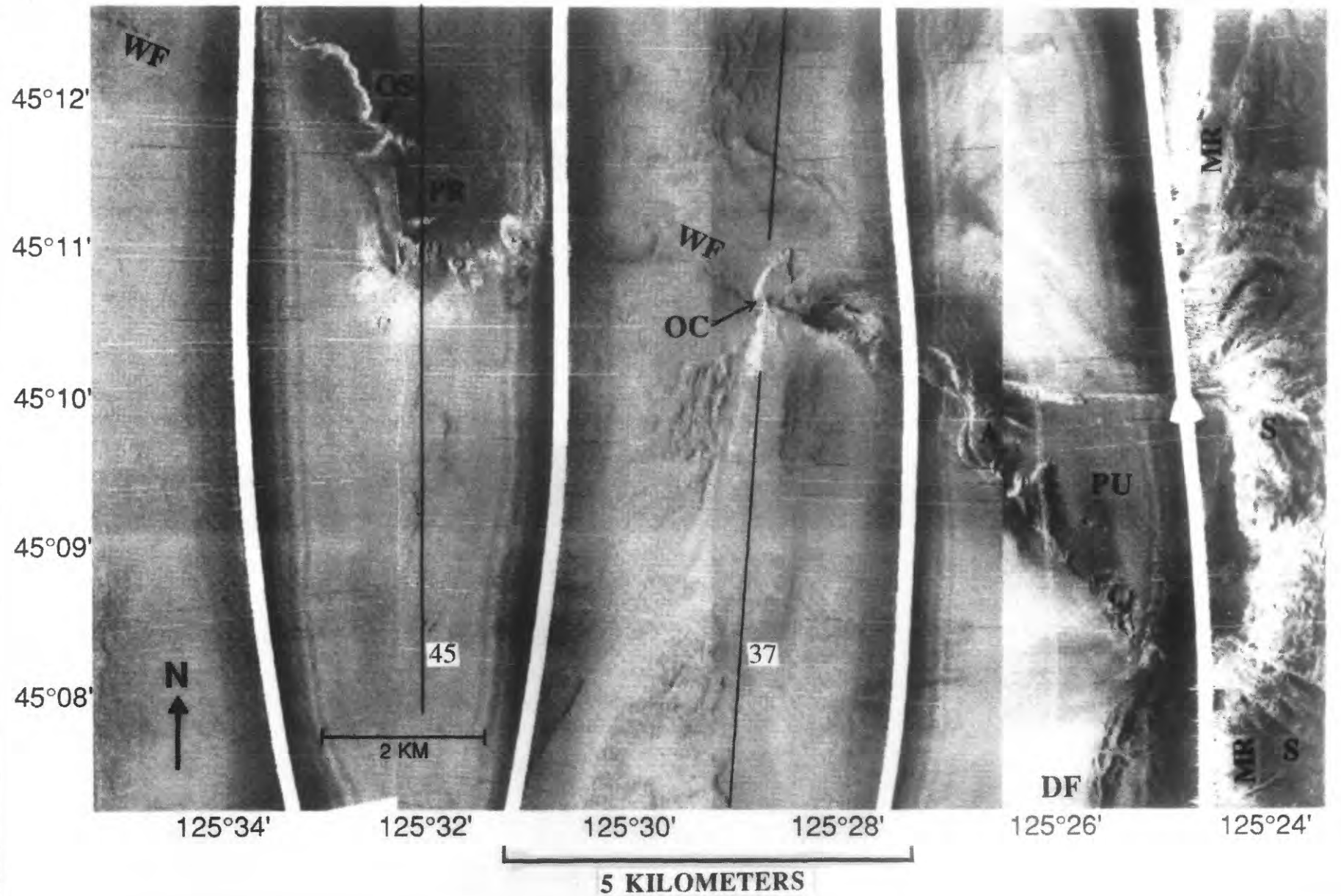
WF
CS
PB
WF
OC
MR
S
PU
DF
MR
S
45
37
N
2 KM
45°12'
45°11'
45°10'
45°09'
45°08'
125°34'
125°32'
125°30'
125°28'
125°26'
125°24'
5 KILOMETERS

Figure 6

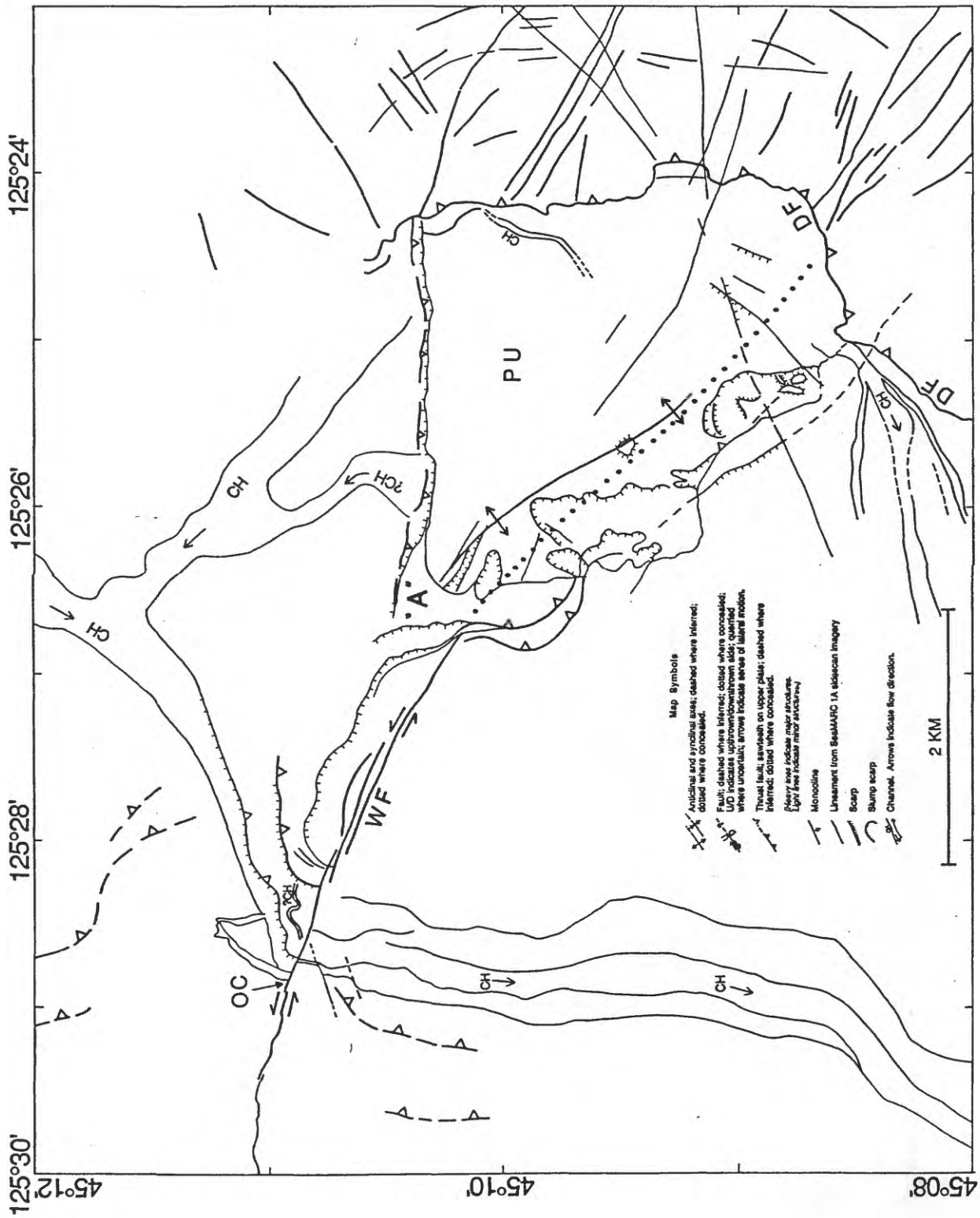
125°24'
125°26'
125°28'
125°30'
45°12'
45°10'
45°08'
PU
DF
DF
CH
2CH
CH
CH
CH
CH
CH
A
A'
WF
OC
Map Symbols
Anticlinal and synclinal axes; dashed where inferred; dotted where concealed.
Fault; dashed where inferred; dotted where concealed; U/D indicates upthrown/downthrown side; queried where uncertain; arrows indicate sense of slip/tilt motion.
Thrust fault; sawteeth on upper plate; dashed where inferred; dotted where concealed.
Heavy lines indicate major structures.
Light lines indicate minor structures.
Monocline
Lineament from SeaMARC 1A sidescan imagery
Scarp
Slump scarp
Channel. Arrows indicate flow direction.
2 KM

Figure 7

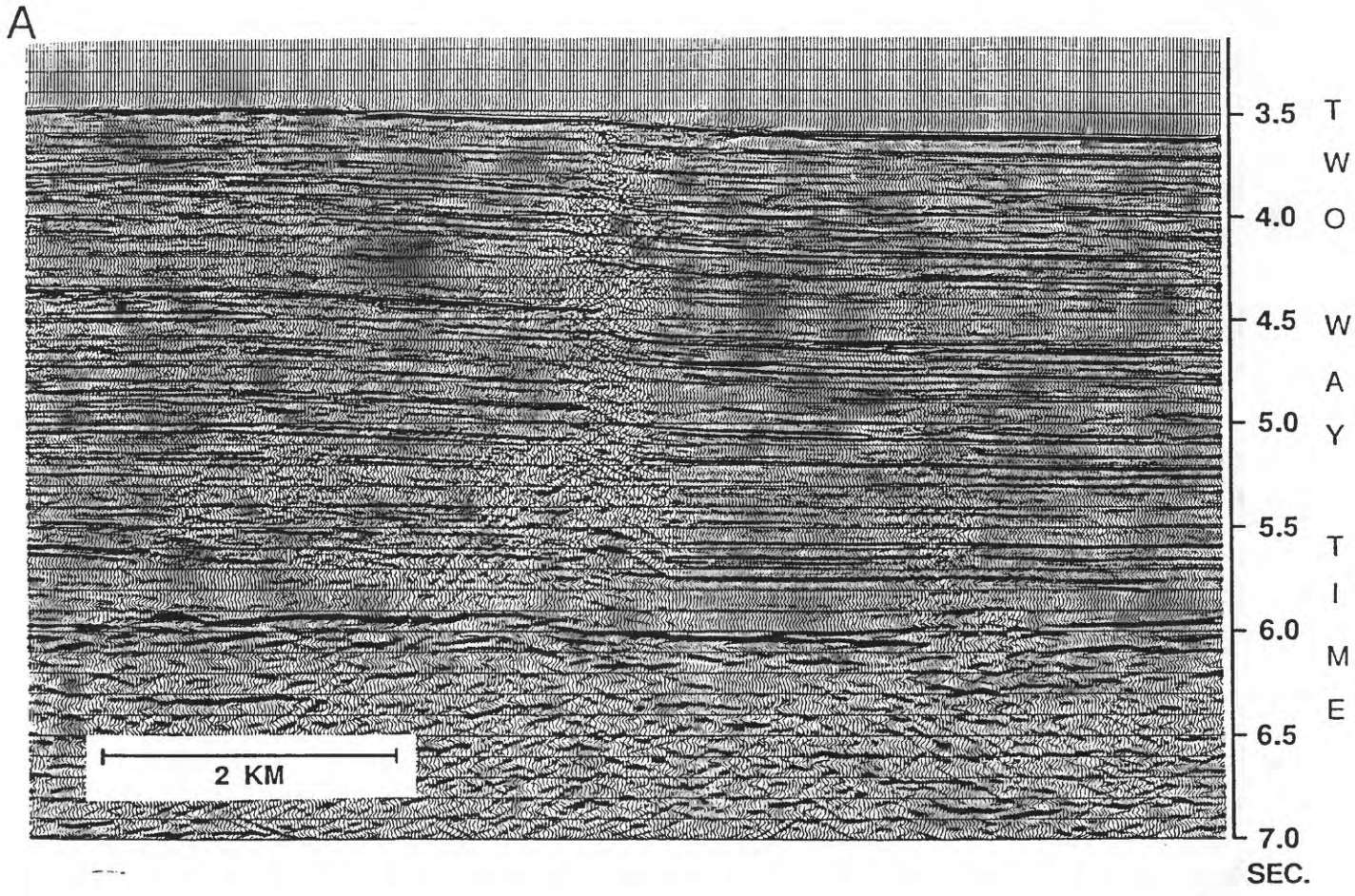
A
3.5
4.0
4.5
5.0
5.5
6.0
6.5
7.0
SEC.
TWO WAY TIME
2 KM

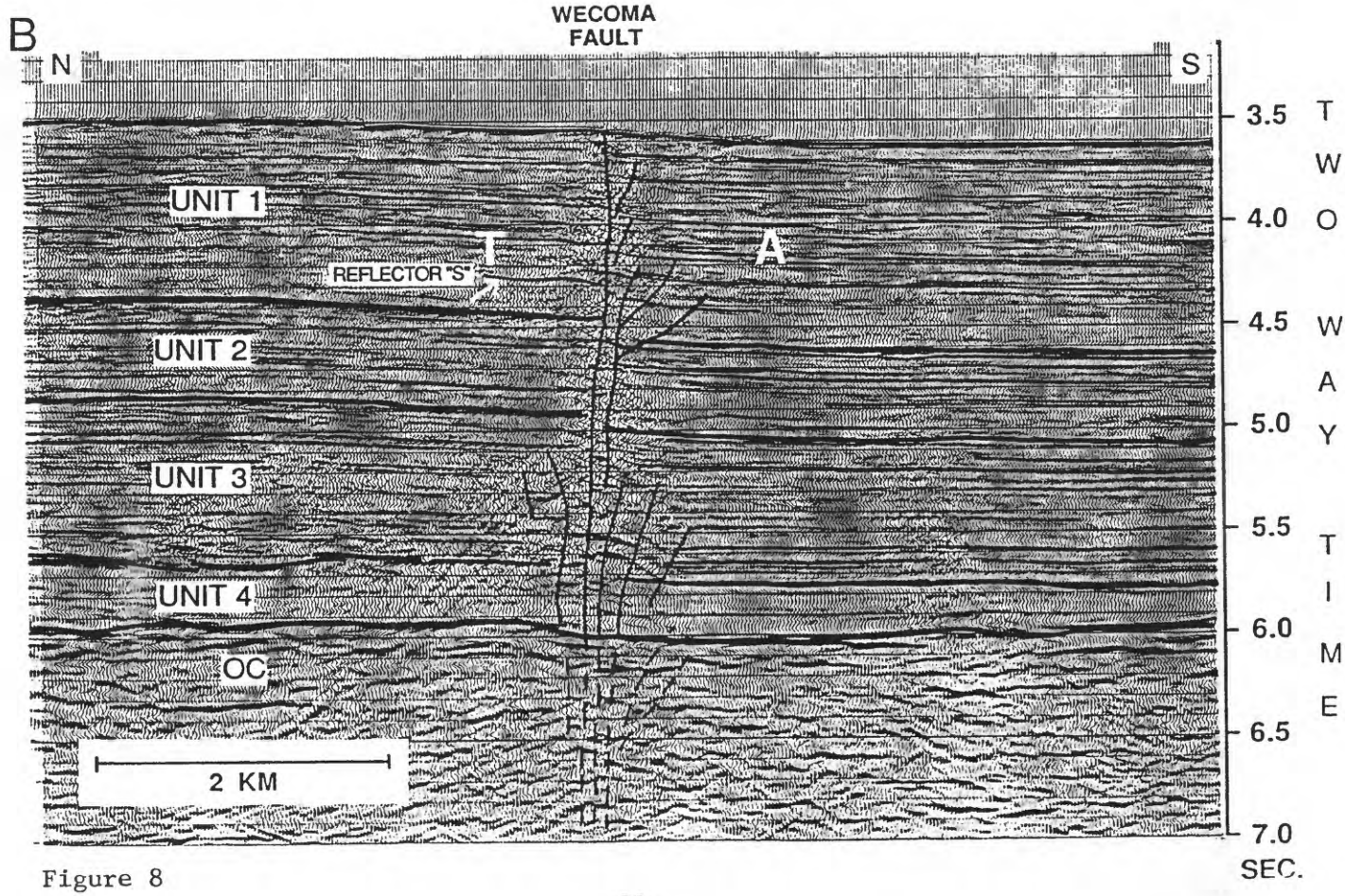
B
WECOMA FAULT
N
S
UNIT 1
UNIT 2
UNIT 3
UNIT 4
OC
REFLECTOR "S"
T
A
2 KM
3.5
4.0
4.5
5.0
5.5
6.0
6.5
7.0
SEC.
TWO WAY TIME

Figure 8

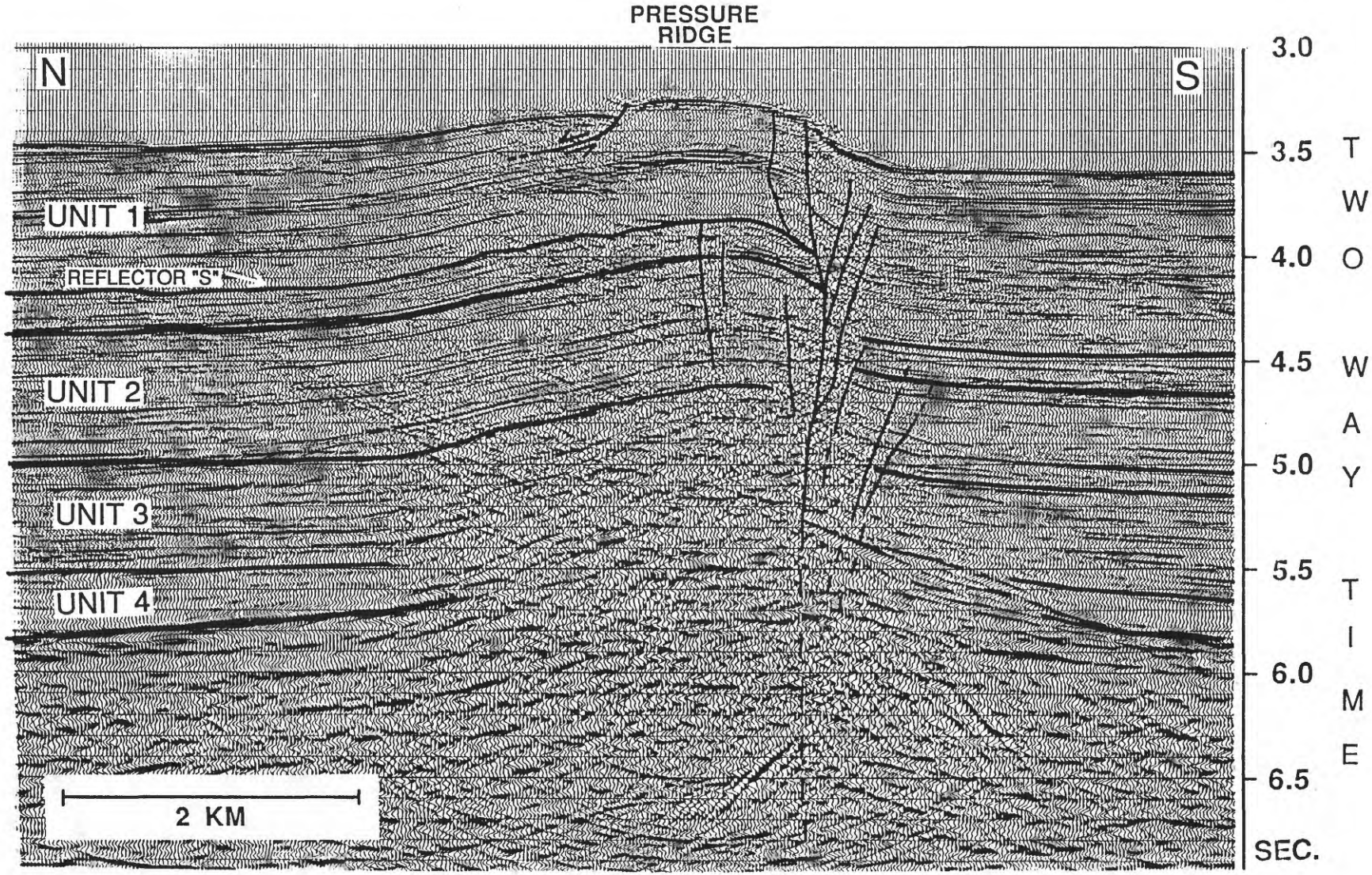
PRESSURE
RIDGE
N
S
UNIT 1
REFLECTOR "S"
UNIT 2
UNIT 3
UNIT 4
2 KM
3.0
3.5
4.0
4.5
5.0
5.5
6.0
6.5
SEC.
TWO WAY TIME

Figure 9

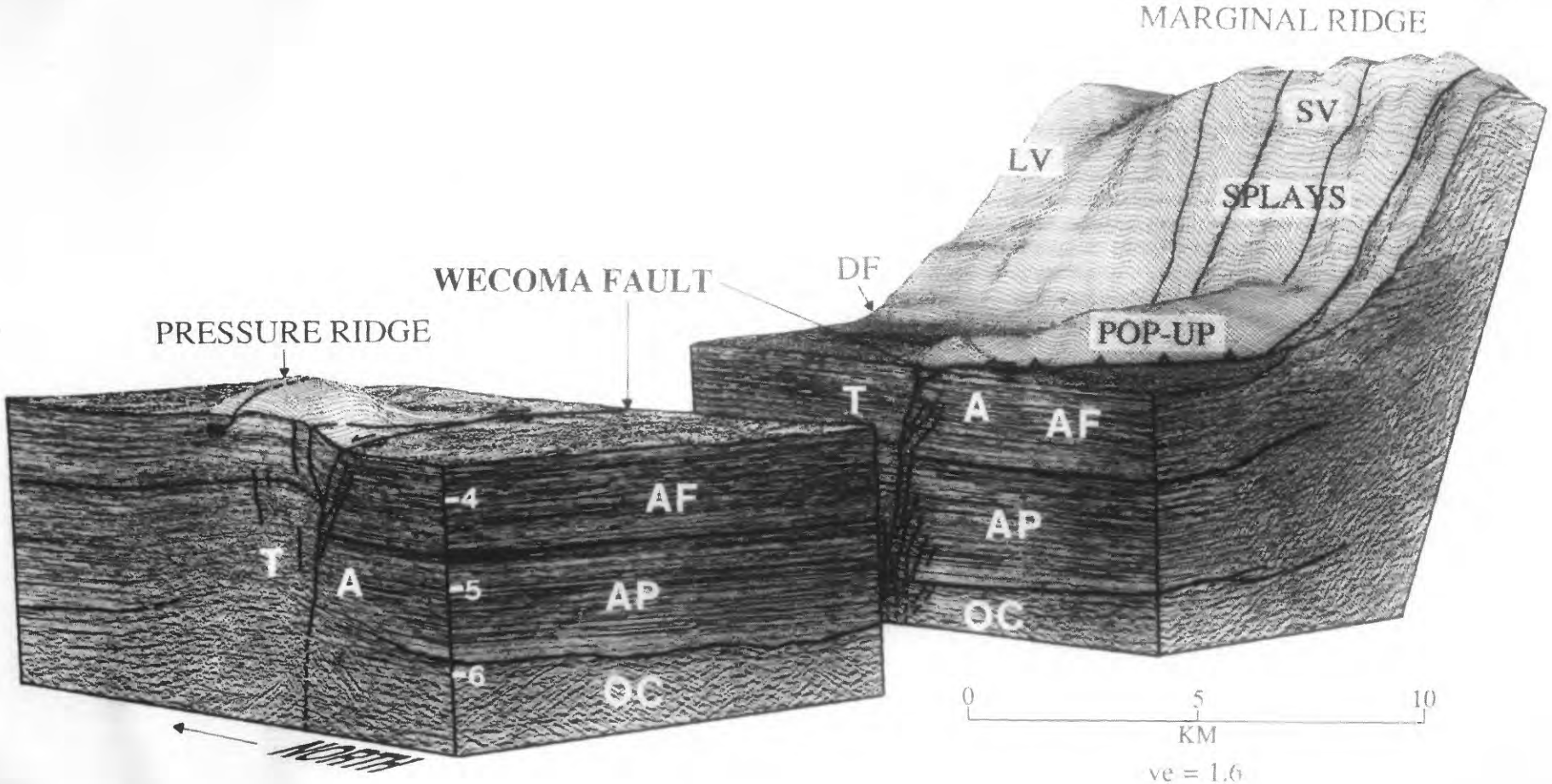
MARGINAL RIDGE
SV
LV
SPLAYS
WECOMA FAULT
DF
POP-UP
PRESSURE RIDGE
T
A
AF
-4
AF
T
A
-5
AP
AP
OC
-6
OC
NORTH
0
5
10
KM
ve = 1.6

Figure 10

Figure 11

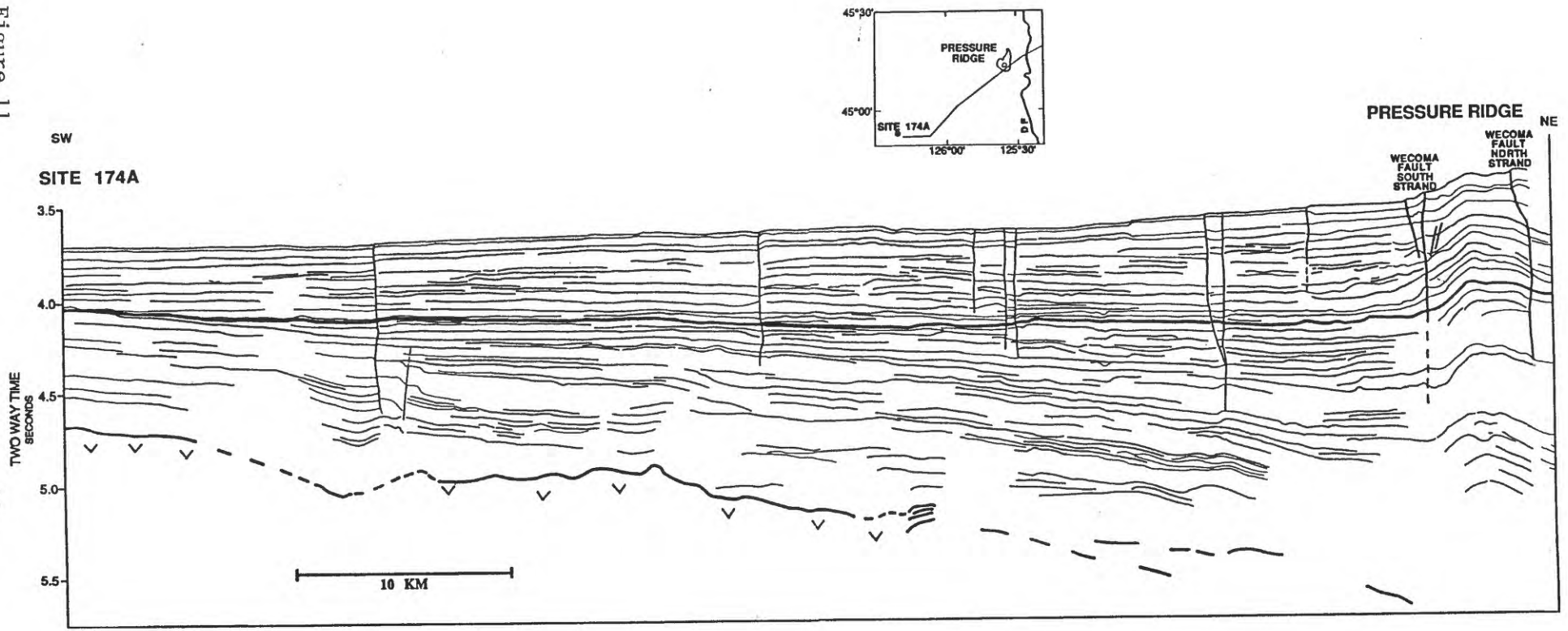
45°30'
PRESSURE RIDGE
45°00'
SITE 174A
126°00'
125°30'
SW
SITE 174A
PRESSURE RIDGE
NE
WECOMA FAULT SOUTH STRAND
WECOMA FAULT NORTH STRAND
3.5
4.0
4.5
5.0
5.5
TWO WAY TIME SECONDS
10 KM

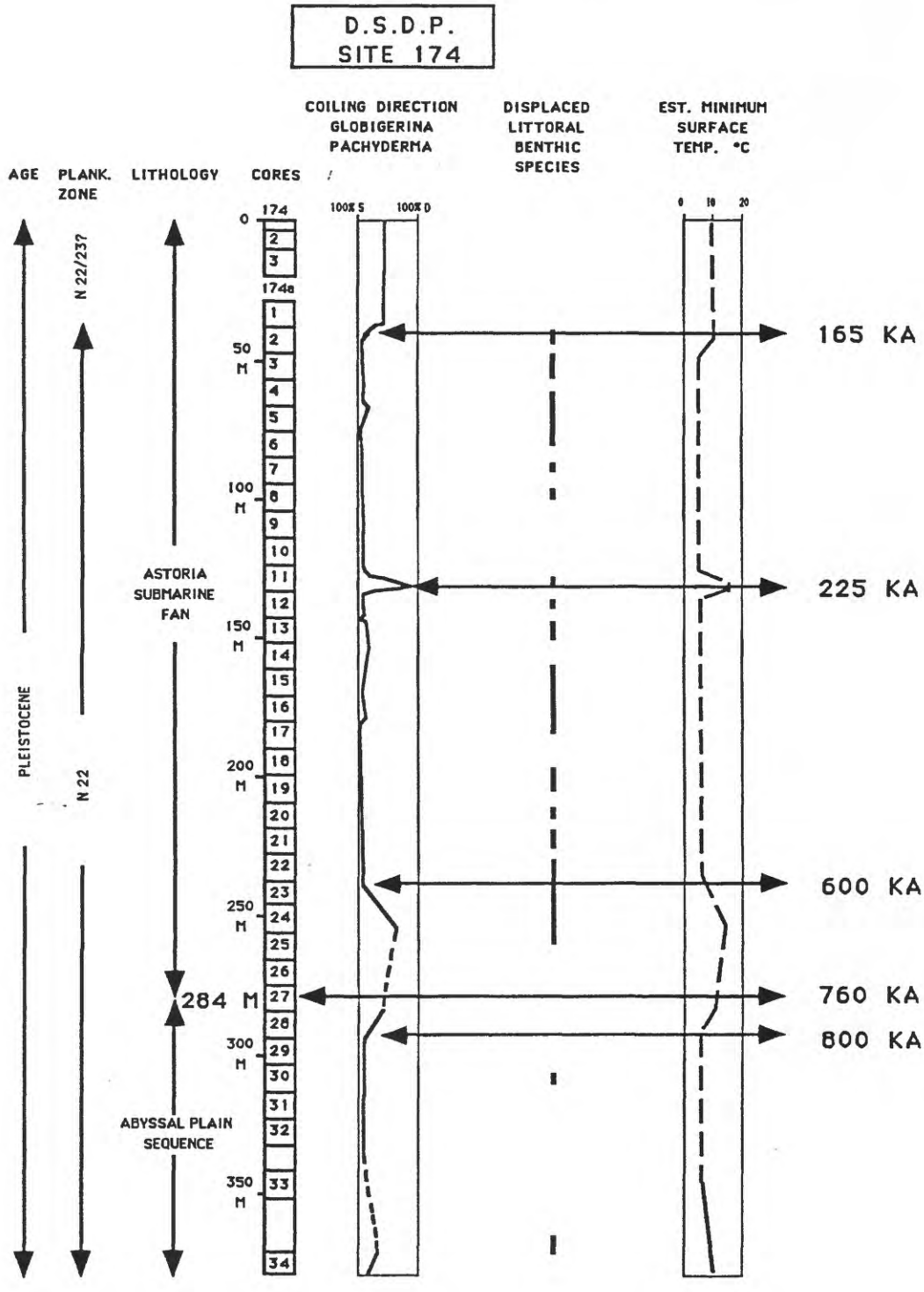
D.S.D.P.
SITE 174
COILING DIRECTION
GLOBIGERINA
PACHYDERMA
DISPLACED
LITTORAL
BENTHIC
SPECIES
EST. MINIMUM
SURFACE
TEMP. °C
AGE
PLANK.
ZONE
LITHOLOGY
CORES
100% S
100% D
0
10
20
PLEISTOCENE
N 22/23?
N 22
ASTORIA
SUBMARINE
FAN
ABYSSAL PLAIN
SEQUENCE
284 M
165 KA
225 KA
600 KA
760 KA
800 KA

Figure 12

SE
NW
5.5 KM
UNIT 1
UNIT 2
UNIT 3
UNIT 4
UNIT 1
UNIT 2
UNIT 3
UNIT 4
PRESENT
POSITION
PRE-FAULT
POSITION
600 KA

Figure 13

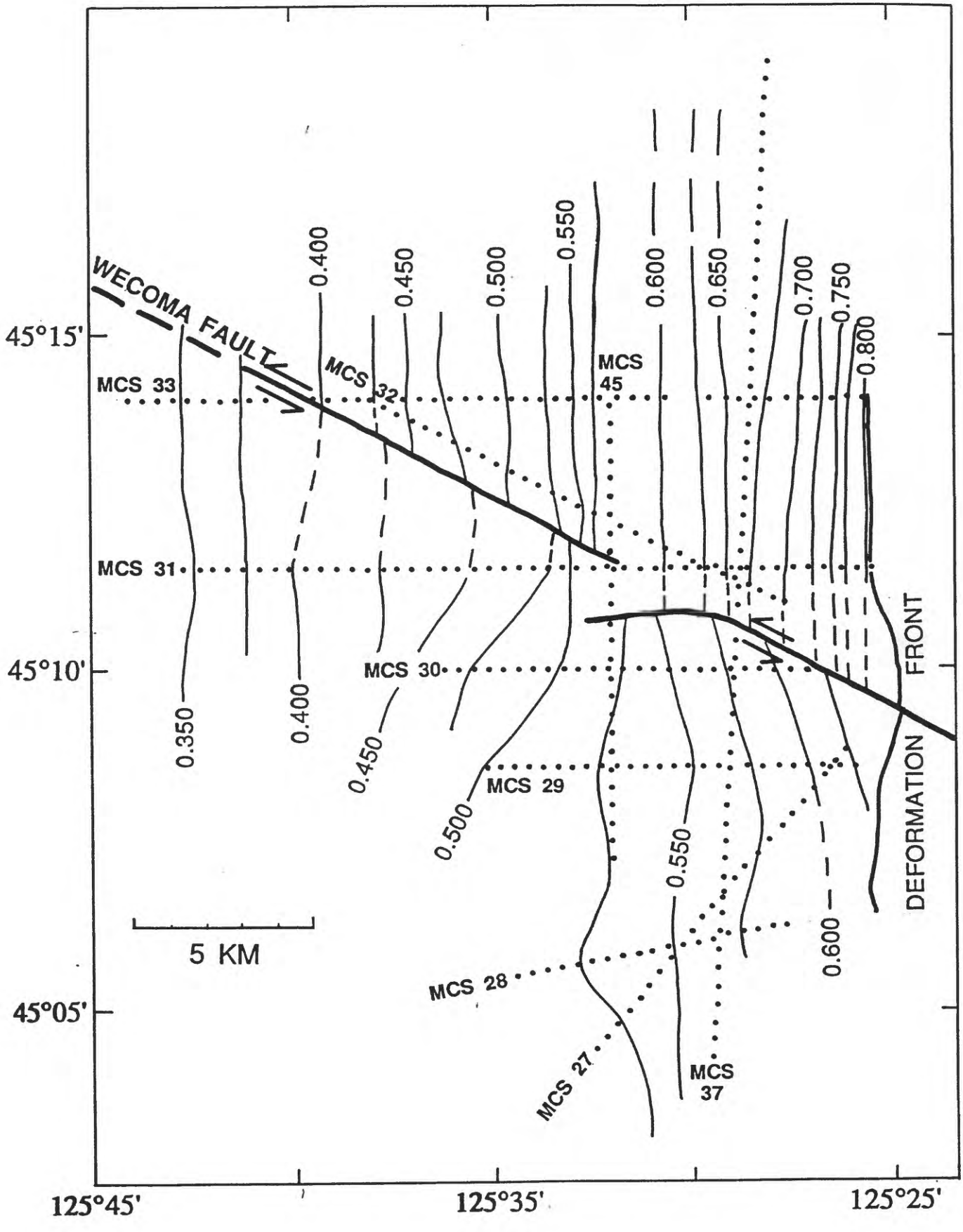
WECOMA FAULT
MCS 33
MCS 32
MCS 31
MCS 30
MCS 29
MCS 28
MCS 27
MCS 45
MCS 37
0.350
0.400
0.450
0.500
0.550
0.600
0.650
0.700
0.750
0.800
DEFORMATION FRONT
5 KM
45°15'
45°10'
45°05'
125°45'
125°35'
125°25'

Figure 14

Slump
400 m
WF
N
Axis
Channel
Offset
Channel
Channel
Wall
Abyssal Plain
Fault
azimuth
292°

Figure 15

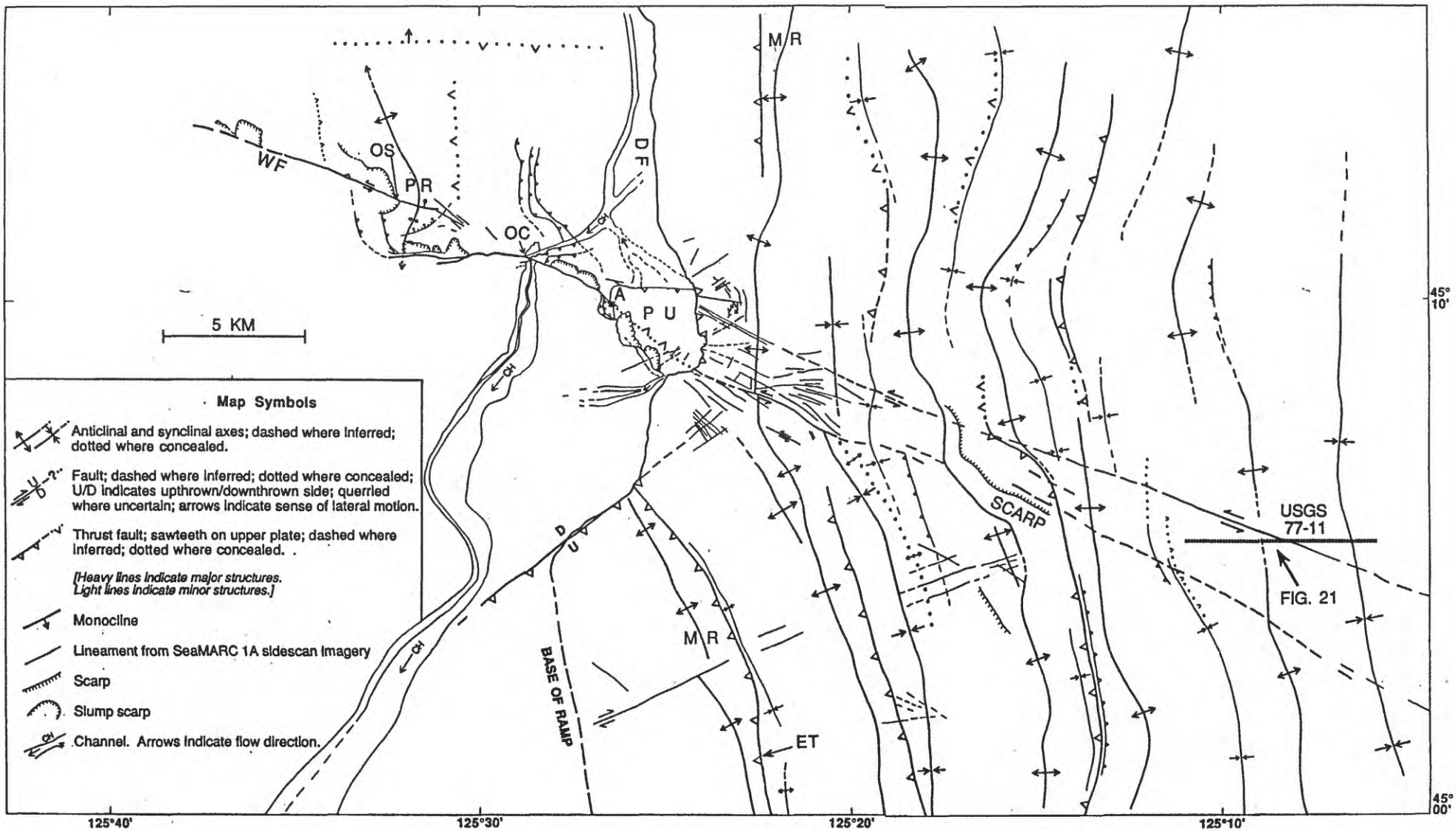
WF
OS
PR
OC
DF
CH
APU
M R
5 KM
Map Symbols
Anticlinal and synclinal axes; dashed where inferred; dotted where concealed.
Fault; dashed where inferred; dotted where concealed; U/D indicates upthrown/downthrown side; querried where uncertain; arrows indicate sense of lateral motion.
Thrust fault; sawteeth on upper plate; dashed where inferred; dotted where concealed.
[Heavy lines indicate major structures. Light lines indicate minor structures.]
Monocline
Lineament from SeaMARC 1A sidescan imagery
Scarp
Slump scarp
Channel. Arrows indicate flow direction.
DU
BASE OF RAMP
ET
SCARP
USGS 77-11
FIG. 21
45° 10'
45° 00'
125°40'
125°30'
125°20'
125°10'

Figure 16

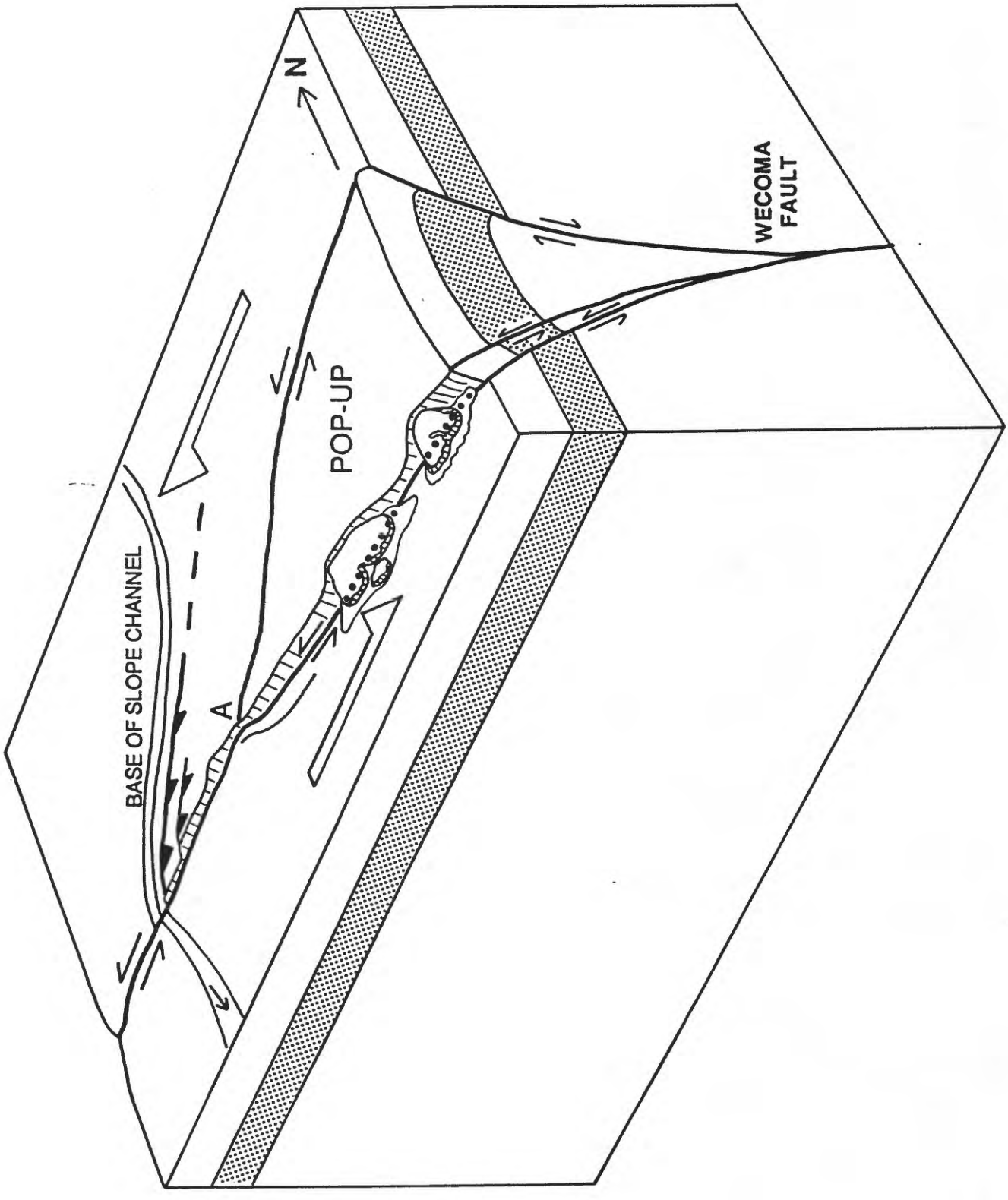

Figure 17

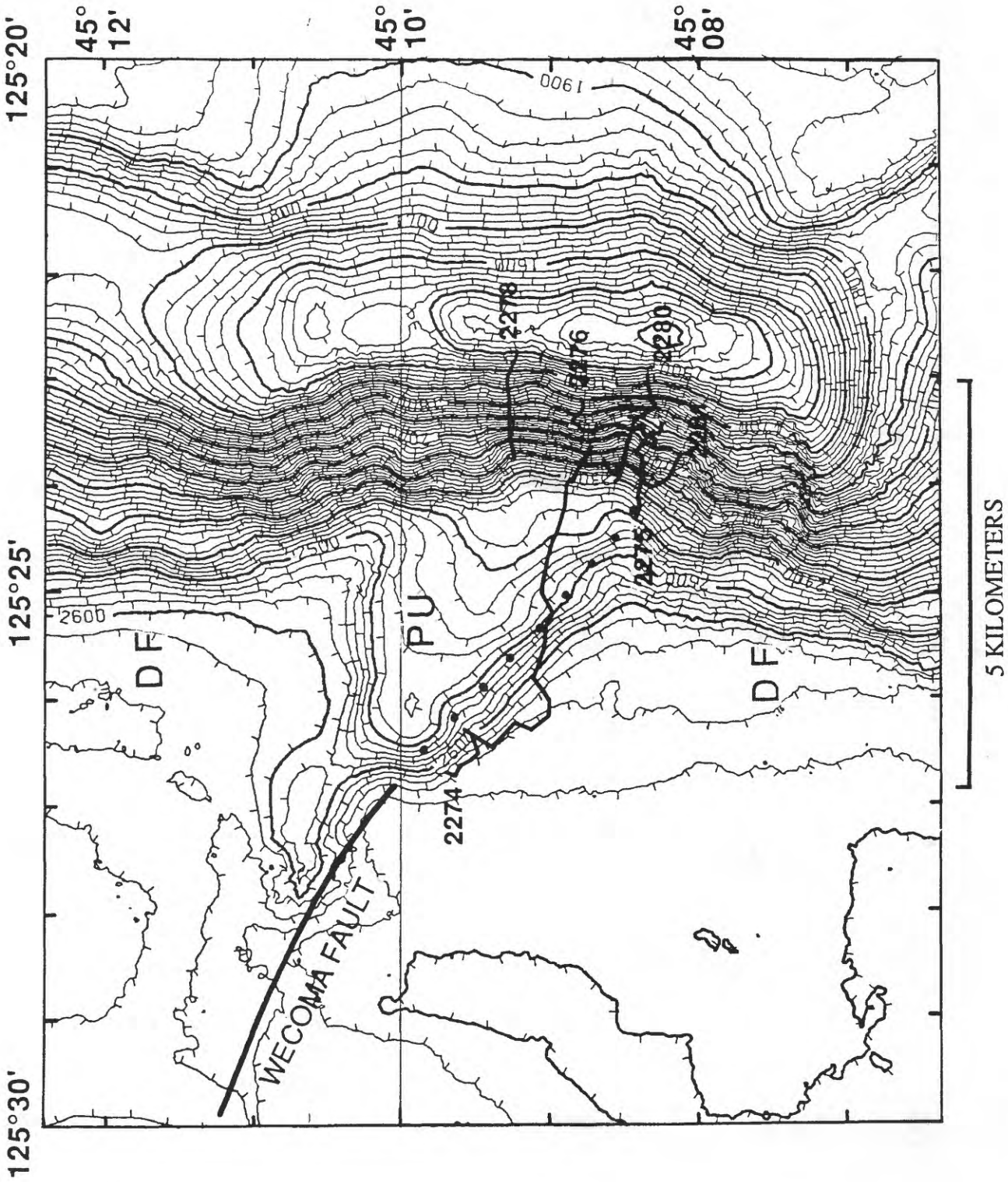
125°20'
125°25'
125°30'
45° 12'
45° 10'
45° 08'
1900
2600
2278
2276
2280
2274
WECOMA FAULT
D F
P U
D F
5 KILOMETERS

Figure 18

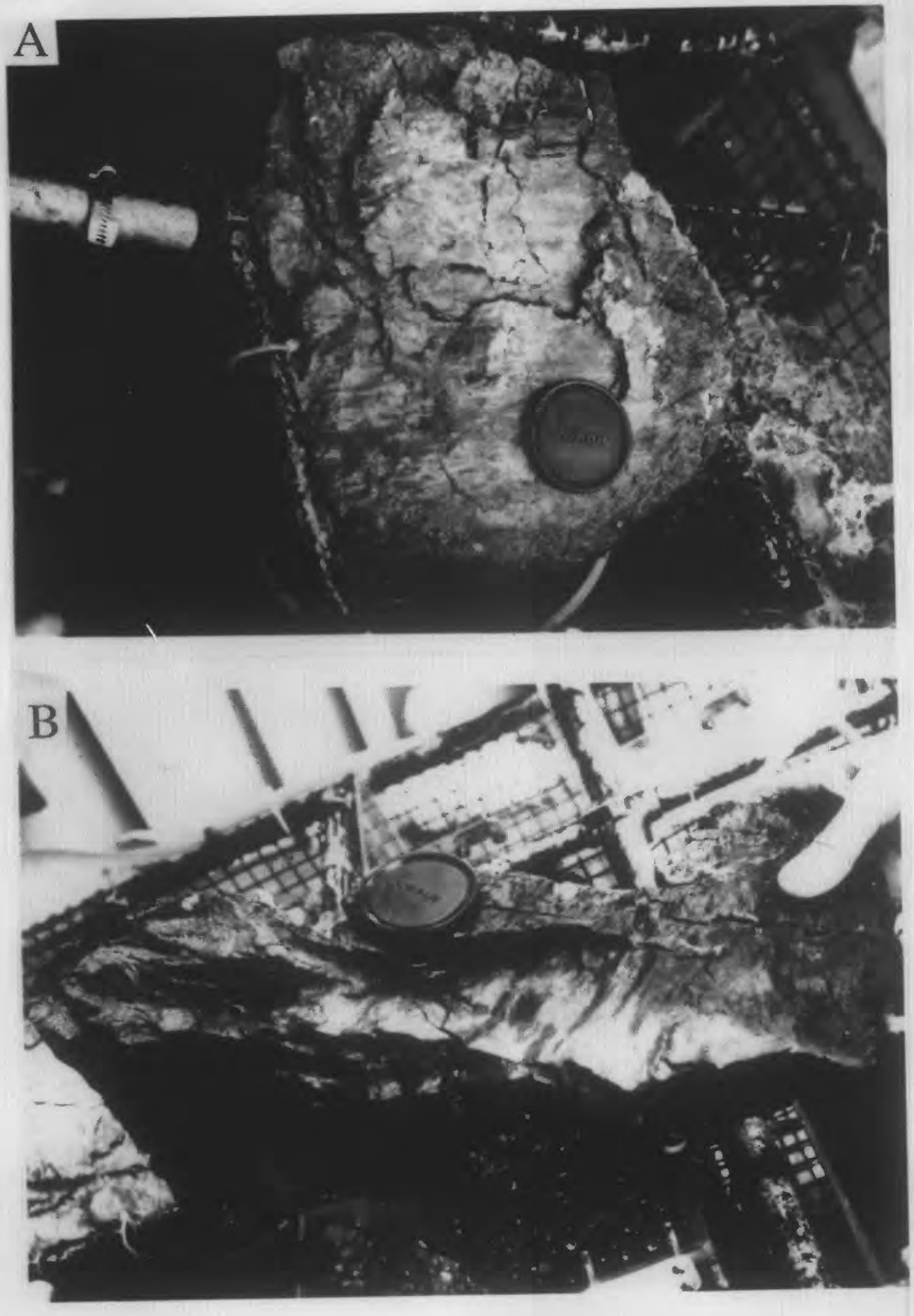

Figure 19

Figure 20 A

125° 10'
125° 15'
125° 20'
125° 25'
45° 10'
45° 05'
N
1 KM
SCARP
WF
B
MR
SPLAYS
RIDGE
OFFSET
WF

Figure 20 B

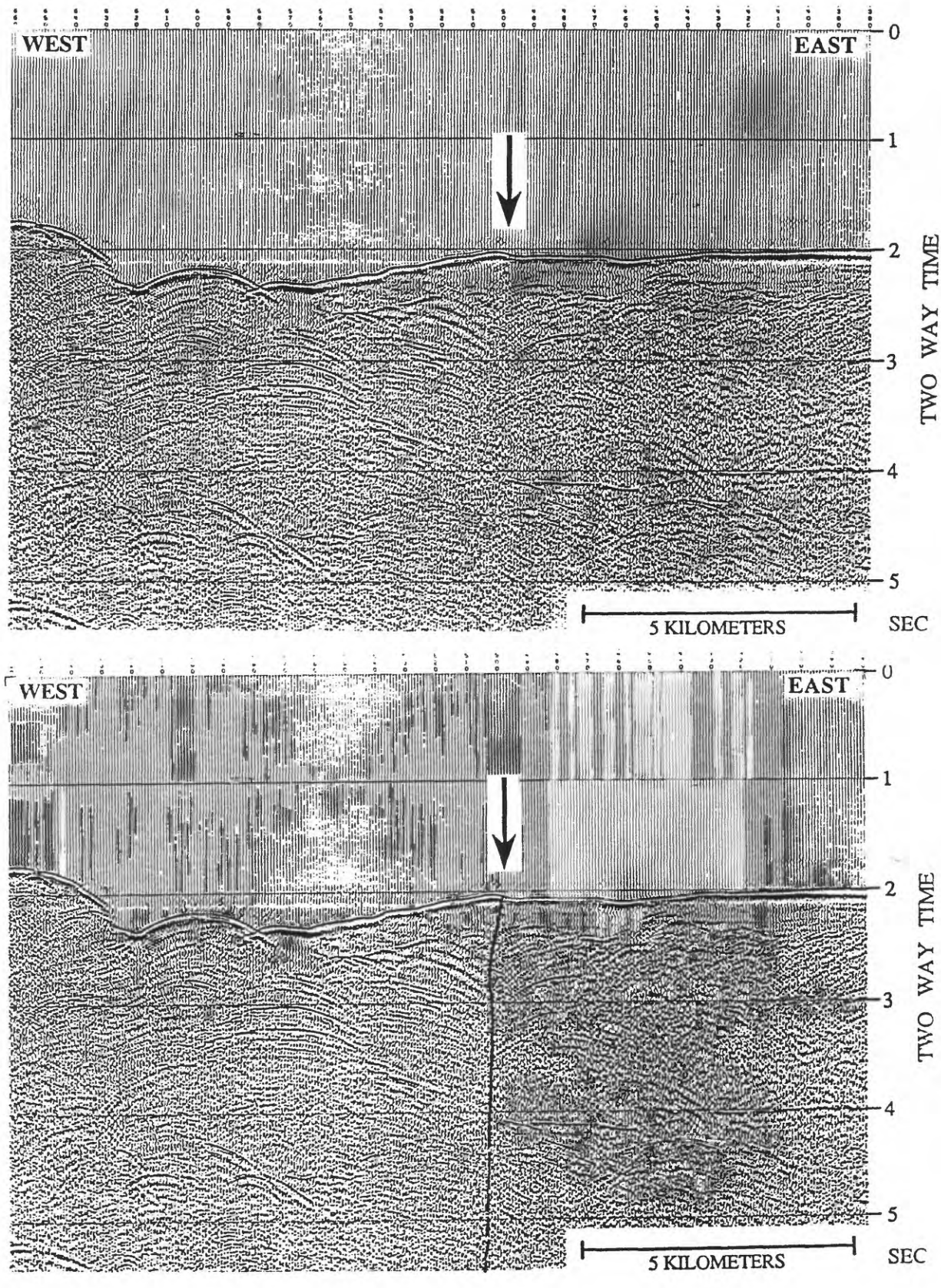
WEST
EAST
0
1
2
3
4
5
TWO WAY TIME
5 KILOMETERS
SEC
WEST
EAST
0
1
2
3
4
5
TWO WAY TIME
5 KILOMETERS
SEC

Figure 21

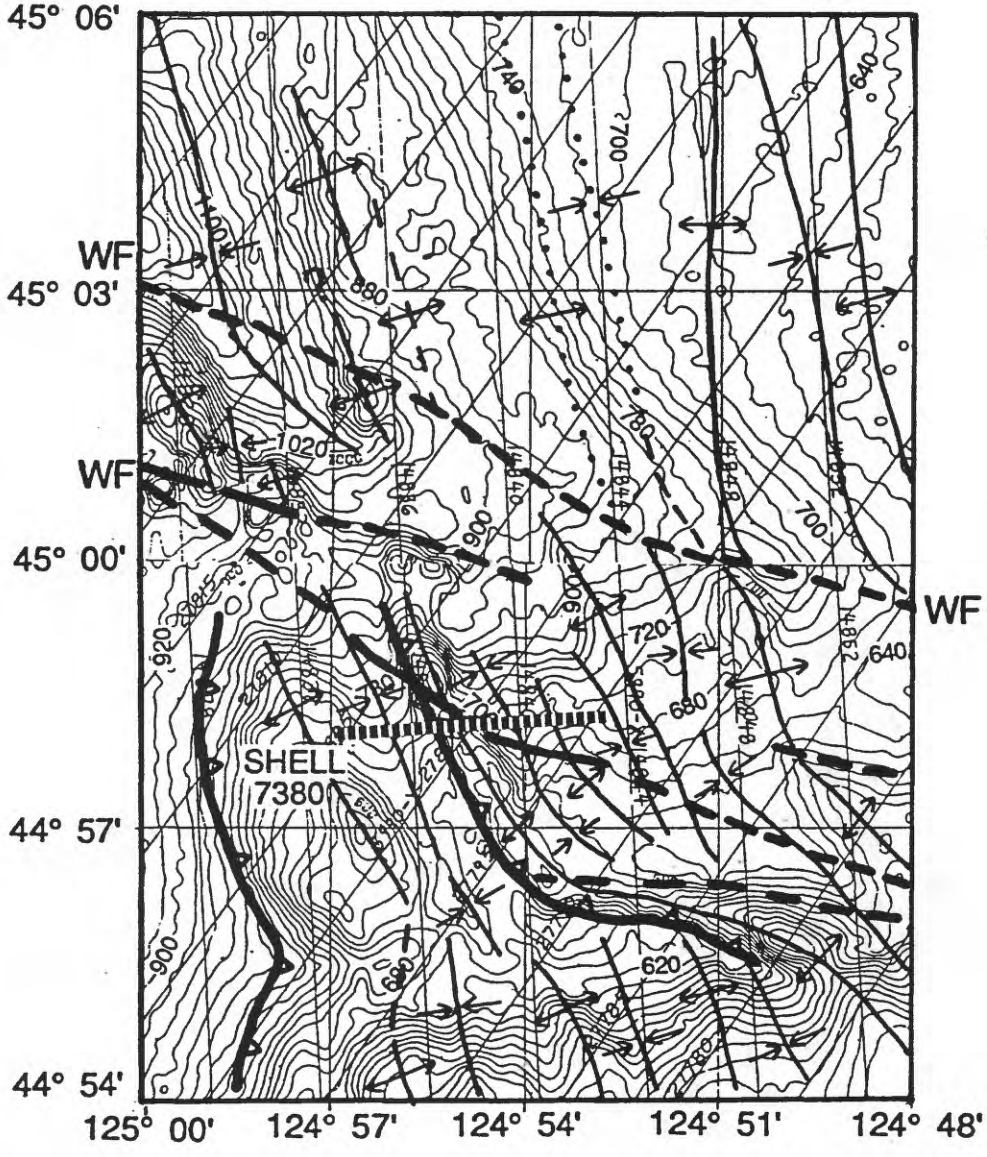
45° 06'
WF
45° 03'
WF
45° 00'
WF
SHELL
7380
44° 57'
44° 54'
125° 00'
124° 57'
124° 54'
124° 51'
124° 48'

Figure 22

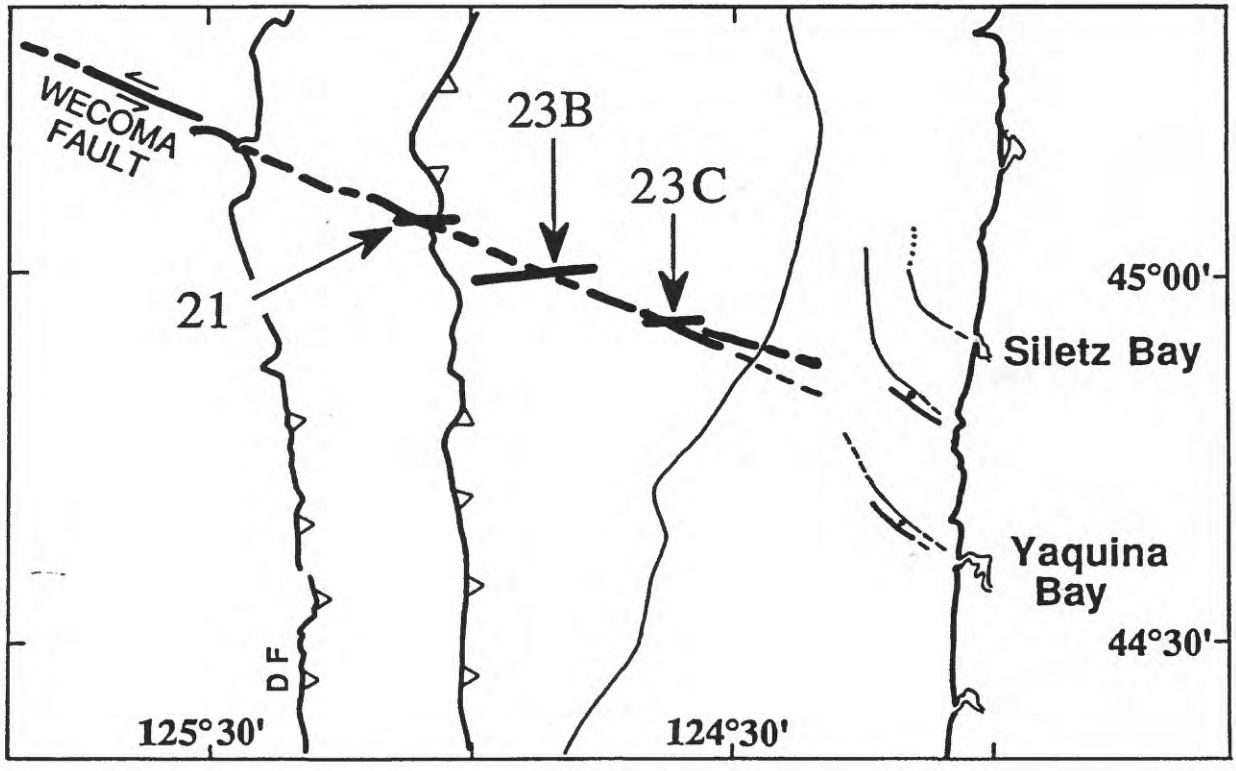
WECOMA
FAULT
23B
23C
21
45°00'
Siletz Bay
Yaquina
Bay
44°30'
DF
125°30'
124°30'

Figure 23 A

Figure 23 B

Fig. 23B

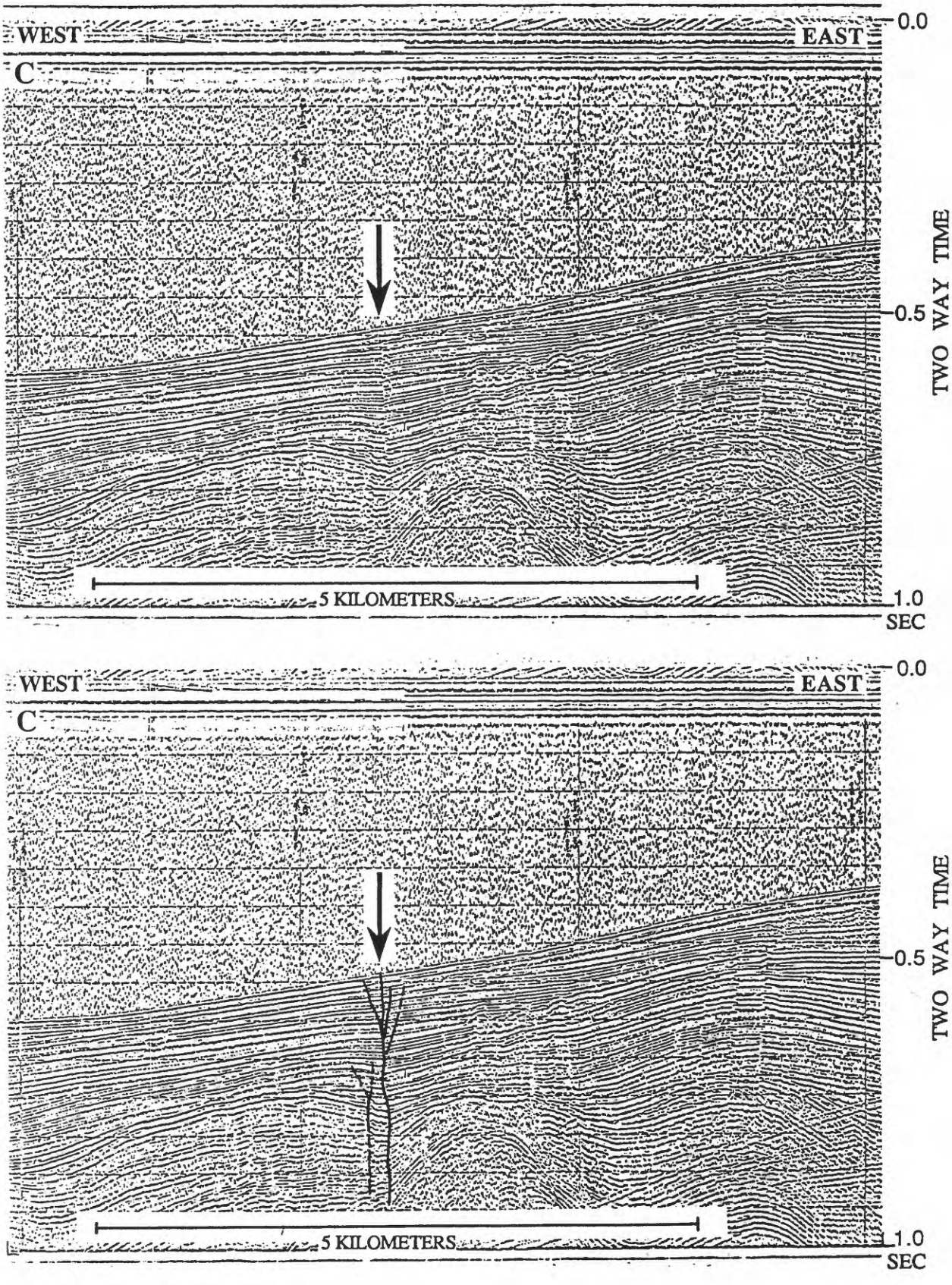
WEST
EAST
C
0.0
0.5
1.0
SEC
TWO WAY TIME
5 KILOMETERS
WEST
EAST
C
0.0
0.5
1.0
SEC
TWO WAY TIME
5 KILOMETERS

Figure 23 C

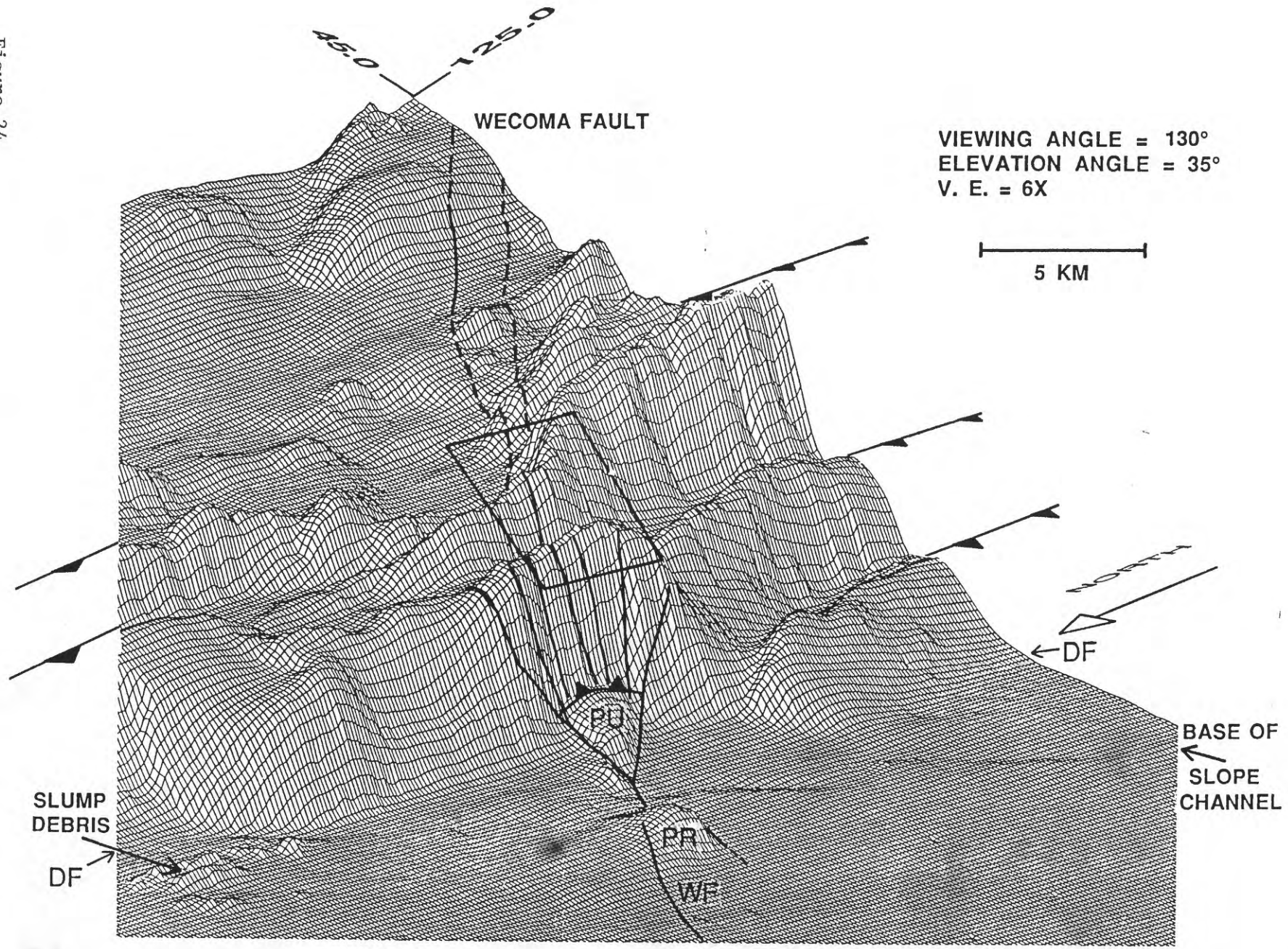
45.0
125.0
WECOMA FAULT
VIEWING ANGLE = 130°
ELEVATION ANGLE = 35°
V. E. = 6X
5 KM
NORTH
DF
PU
BASE OF
SLOPE
CHANNEL
SLUMP
DEBRIS
DF
PR
WF

Figure 24

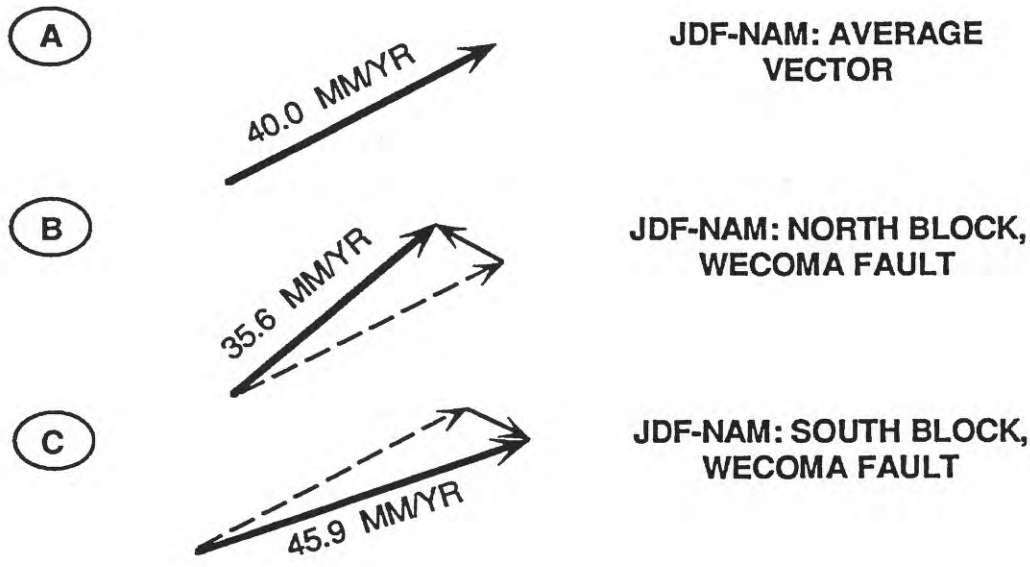
A
40.0 MM/YR
JDF-NAM: AVERAGE VECTOR
B
35.6 MM/YR
JDF-NAM: NORTH BLOCK, WECOMA FAULT
C
45.9 MM/YR
JDF-NAM: SOUTH BLOCK, WECOMA FAULT

Figure 25